Multi-model comparison of the volcanic sulfate deposition from the 1815 eruption of Mt. Tambora

Lauren Marshall[1], Anja Schmidt[1], Matthew Toohey[2,3], Ken S. Carslaw[1], Graham W. Mann[1,4], Michael Sigl[5], Myriam Khodri[6], Claudia Timmreck[3], Davide Zanchettin[7], William Ball[8,9], Slimane Bekki[10], James S.A. Brooke[11], Sandip Dhomse[1], Colin Johnson[12], Jean-Francois Lamarque[13], Allegra LeGrande[14], Michael J. Mills[13], Ulrike Niemeier[3], Virginie Poulain[6], Alan Robock[15], Eugene Rozanov[8,9], Andrea Stenke[8], Timofei Sukhodolov[9], Simone Tilmes[13], Kostas Tsigaridis[14], Fiona Tummon[8]

[1]Institute for Climate and Atmospheric Science, School of Earth and Environment, University of Leeds, UK
[2] GEOMAR Helmholtz Centre for Ocean Research Kiel, Kiel, Germany
[3] Max Planck Institute for Meteorology, Hamburg, Germany
[4]National Centre for Atmospheric Science, University of Leeds, UK
[5]Laboratory of Environmental Chemistry, Paul Scherrer Institut, 5232 Villigen, Switzerland
[6]IRD/IPSL/Laboratoire d'Océanographie et du Climat, Paris, France
[7]Department of Environmental Sciences, Informatics and Statistics, University Ca' Foscari of Venice, Mestre, Italy
[8]Institute for Atmospheric and Climate Science, ETH Zurich, Zurich, Switzerland
[9]PMOD/WRC, Davos, Switzerland
[10]LATMOS-IPSL, Université UPMC/Paris-Sorbonne, Université UVSQ/Paris Saclay, CNRS/INSU, Paris, France
[11]School of Chemistry, University of Leeds, UK
[12]Met Office Hadley Centre, Exeter, UK
[13]Atmospheric Chemistry Observations and Modeling Laboratory, National Center for Atmospheric Research, Boulder, CO, USA
[14]NASA Goddard Institute for Space Studies and Center for Climate Systems Research, Columbia University, New York, NY, USA
[15]Department of Environmental Sciences, Rutgers University, New Brunswick, NJ, USA

Correspondence to: Lauren Marshall (eelrm@leeds.ac.uk)

Abstract. The eruption of Mt. Tambora in 1815 was the largest volcanic eruption of the past 500 years. The eruption had significant climatic impacts, leading to the 1816 'Year Without a Summer' and remains a valuable event from which to understand the climatic effects of large stratospheric volcanic sulfur dioxide injections. The eruption also resulted in one of the strongest and most easily identifiable volcanic signals in polar ice cores, which are widely used to reconstruct the timing

5   and atmospheric sulfate loading of past eruptions. As part of the Model Intercomparison Project on the climatic response to Volcanic forcing (VolMIP), four state-of-the-art global aerosol models simulated this eruption. We analyse both simulated background (no Tambora) and volcanic (with Tambora) sulfate deposition to polar regions and compare to ice core records. Background sulfate deposition is of similar magnitude across all models and compares well to ice core records. However, volcanic sulfate deposition varies in timing, spatial pattern and magnitude between the models. Mean simulated deposited

10   sulfate on Antarctica ranges from 19 to 264 kg km^{-2}, and on Greenland from 31 to 194 kg km^{-2}, as compared to the mean ice core-derived estimates of roughly 40-50 kg km^{-2}, for both Greenland and Antarctica. The ratio of the hemispheric atmospheric sulfate aerosol burden after the eruption to the average ice sheet deposited sulfate varies between models by up to a factor of 15. Sources of this inter-model variability include differences in both the formation and the transport of sulfate aerosol. Our results highlight the uncertainties and difficulties in deriving historic volcanic aerosol radiative forcing of

15   climate, based on measured volcanic sulfate in polar ice cores.

1 Introduction

Mt. Tambora in Indonesia (8.2°S, 118.0°E) erupted in April 1815 (e.g. Oppenheimer, 2003) and had a considerable impact on climate, leading to widespread tropical and Northern Hemisphere mean cooling of ~1°C and a 'Year Without a Summer' in 1816 (e.g. Raible et al., 2016). Volcanic sulfate aerosol, produced from the oxidation of sulfur dioxide (SO_2)

20   emitted into the atmosphere by volcanoes, is transported throughout the atmosphere and deposited to the surface by both wet and dry processes, some of which is eventually incorporated into polar ice (e.g. Robock, 2000). Bipolar volcanic sulfate deposition signals are presumed to result from tropical eruptions, whereby sulfur entering the tropical stratosphere is converted to sulfate aerosol, which is transported globally by the Brewer-Dobson circulation (e.g. Trepte et al., 1993; Langway et al., 1995; Robock, 2000; Gao et al., 2007). Polar ice core deposition signals typically start around 0.5-1 year

25   after a large tropical eruption and remain elevated for approximately 2 - 3 years (Robock and Free, 1995; Sigl et al., 2015). Throughout the last 2500 years, polar ice core records show over 200 sulfate spikes, which have been used to estimate the timing, evolution and magnitude of radiative forcing of climate caused by volcanic eruptions during this period (Sigl et al., 2015). The 1815 eruption of Mt. Tambora produced the 6th largest bipolar sulfate signal in the last 2500 years (Sigl et al., 2015).

30   Determining the stratospheric aerosol properties of the 1815 Mt. Tambora eruption such as spatial extent of the sulfate aerosol cloud, aerosol optical depth and aerosol size distribution bears substantial uncertainties, which ultimately affects the quantification of its climatic impacts using climate models. As part of the Model Intercomparison Project on the

climatic response to volcanic forcing (VolMIP) (Zanchettin et al., 2016), which is a Coupled Model Intercomparison Project Phase 6 (CMIP6) endorsed activity (Eyring et al., 2016), coordinated simulations of the 1815 eruption of Mt. Tambora were performed with four state-of-the-art global aerosol models. Our study, motivated by the uncertainty that remains in the climatic forcing from this eruption, investigates the sources of uncertainty in the sulfate deposition to polar regions in these

5 simulations, and discusses implications for reconstructions of historic volcanic forcing.

Previous reconstructions of volcanic sulfate aerosol properties used to force climate models scaled the average sulfate deposited on Antarctica and Greenland to the hemispheric atmospheric sulfate aerosol burden (e.g. Gao et al., 2007; Crowley & Untermann, 2013; Sigl et al., 2015). Scaling factors (ratios of the hemispheric sulfate aerosol burden to the sulfate deposited at the poles) were based on the ratio of these two quantities as observed after the eruption of Mt. Pinatubo

10 in 1991 and from the estimated atmospheric burden and measured deposited radioactive material after nuclear bomb tests. Previous climate model simulations of the ratio between atmospheric sulfate burden and polar deposited sulfate and were also used to derive the scaling factors (Gao et al., 2007; 2008). These scaling factors may not hold for larger eruptions where volcanic sulfate aerosol particles can grow larger, increasing their sedimentation rate (e.g. Pinto et al., 1989; Timmreck et al., 2009). Toohey et al. (2013) also found that differences in the dynamical response to large-magnitude eruptions changed the

15 spatial distribution of the deposited sulfate. Furthermore, available ice core measurements are not evenly distributed over both ice caps, and large spatial variations in the sulfate deposition fluxes can exist between individual ice cores due to differences in local accumulation rates and sulfate redistribution by snow drift (Clausen and Hammer, 1988; Zielinski et al., 1997; Cole-Dai et al., 1997, 2000; Wolff et al., 2005; Gao et al., 2006, 2007). It is therefore important that a range of ice core records from different geographical regions is used to estimate the average volcanic sulfate deposited on each ice cap.

20 Previous studies using only a few ice cores to reconstruct volcanic forcing histories may be biased (e.g. Zielinski, 1995; Zielinski et al., 1996; Crowley, 2000), although it has been demonstrated that deposition fluxes derived from single ice cores at high accumulation sites are representative of total ice sheet deposition (Toohey and Sigl, 2017). Gao et al. (2007), who analysed 44 ice cores to investigate the spatial distribution of volcanic sulfate deposition during the last millennium, found larger average deposited sulfate on Greenland (mean deposition of 59 kg km^{-2}, using 22 ice cores) than on Antarctica (mean

25 deposition of 51 kg km^{-2}, 17 ice cores) for the eruption of Mt. Tambora. However, Sigl et al. (2015) found, using additional high temporal-resolution ice core records in Antarctica (Sigl et al., 2014), average Antarctic deposited sulfate of 46 kg km^{-2}, and a smaller average deposited sulfate on Greenland of 40 kg km^{-2}, with both averages smaller than the averages provided by Gao et al. (2007). Although in Sigl et al. (2015) the Antarctic average was derived with 17 ice core records, the Greenland average was calculated from only two ice cores (NEEM and NGRIP) compared to the 22 cores used for Greenland in Gao et

30 al. (2007).

Previous modelling studies that have investigated the sulfate deposition from the 1815 eruption of Mt. Tambora have failed to reproduce the magnitude of the measured deposited sulfate on both ice caps compared to ice core records, although the models were able to capture the spatial pattern (Gao et al., 2007; Toohey et al., 2013). Gao et al. (2007) found the model-simulated mean deposited sulfate to be a factor of two greater than the ice core-derived estimate, with average

Antarctic deposited sulfate of 113 kg km^{-2} and smaller Greenland deposited sulfate of 78 kg km^{-2}. Toohey et al. (2013), on the other hand, found higher deposition to Greenland, and although matching the spatial pattern of deposited sulfate on Antarctica remarkably well, found model-simulated mean deposited sulfate to be ~4.7 greater than inferred from ice cores. Differences between simulated and measured deposited sulfate could be caused by inaccuracies in the model representation

5 of several physical processes such as the formation and transport of sulfate aerosol, sedimentation, cross-tropopause transport and deposition processes (e.g. Hamill et al., 1997; SPARC, 2006). Neither of the models used by Toohey et al. (2013) and Gao et al. (2007) included a representation of the Quasi-Biennial Oscillation (QBO), which may significantly impact the initial aerosol dispersion (e.g. Trepte et al., 1993). Furthermore, uncertainties exist in the source parameters used for simulating the eruption in models such as the SO$_2$ emission magnitude and emission height.

10 In general, sulfate deposited on the polar ice caps is only a small fraction of the sulfate deposited globally (e.g. Toohey et al., 2013) and there remains uncertainty surrounding the partitioning of the 1815 Mt. Tambora volcanic sulfate aerosol between both hemispheres. Model results can aid in the interpretation of the ice core estimates, by allowing us to assess the relationship between the simulated atmospheric sulfate aerosol burdens and the simulated deposited sulfate.

In this paper we focus on the model-simulated sulfate deposition and the implications for reconstructions of historic

15 volcanic forcing by analysing the deposited sulfate simulated by four global aerosol models and comparing to ice core records. Section 2 describes the model simulations and ice core records. In section 3 we assess the sulfate deposition simulated under both background (no Tambora) (Sec. 3.1) and volcanically perturbed (with Tambora) conditions (Sec. 3.2) and compare the simulated deposited sulfate to ice core measurements. We investigate the relationship between hemispheric atmospheric sulfate burdens and mean ice sheet deposited sulfate in section 3.3 and explore reasons for model differences in

20 section 4. Conclusions are presented in section 5.

2 Model set-up and ice core data

The four global aerosol models included in this study are listed in Table 1. Three of the four models have modal aerosol schemes in that the aerosol particle size distribution is represented by several log-normal modes. In a sectional scheme the aerosol size distribution is represented by discrete size bins (e.g. SOCOL). A more comprehensive list of model

25 specifications is provided in the supplementary material (Table S1).

The parameters used for the Mt. Tambora simulations are listed in Table 2. Each model simulated the eruption by emitting 60 Tg of SO$_2$ at the approximate location of Mt. Tambora (Table S1), between approximately 22-26 km (see details in Table 2 regarding the injection details for each model) and during the easterly QBO phase. This SO$_2$ emission estimate is based on both petrological and ice core estimates (Self et al., 2004; Gao et al., 2008), however there remains uncertainty

30 regarding the amount of SO$_2$ emitted, which could range between ~30 – 80 Tg SO$_2$ (e.g. Stoffel et al., 2015). Nevertheless, 60 Tg SO$_2$ remains our best estimate. There is also uncertainty in the altitude of the emission and QBO phase due to the lack of observations. Therefore, the injection altitude and QBO phase were chosen to match those of the 1991 Mt. Pinatubo

eruption based on satellite and lidar observations (McCormick and Veiga, 1992; Read et al., 1993; Herzog and Graf, 2010). The eruption was simulated for 24 hours on 1 April.

Sea surface temperatures, greenhouse gas concentrations, tropospheric aerosols and ozone were set to climatological preindustrial settings as defined by each modelling group. The simulations were run for five years and included five ensemble members, except for WACCM, which had three members only. The models include additional species and processes compared to earlier modelling studies of Mt. Tambora (e.g. Gao et al., 2007; Toohey et al., 2013). UKCA for example includes meteoric smoke particles and an internally generated QBO. Model output is in the form of monthly means.

The ice cores used in this analysis are provided in Tables S2-S3. The Antarctic ice cores are the most extensive array of annually resolved cores that have been used to reconstruct historic volcanic forcing (Sigl et al., 2014; 2015). Greenland ice core records have been compiled from several studies (Table S2). Further ice core measurements of the natural background sulfate deposition fluxes were taken from Lamarque et al. (2013).

Sulfate deposition fluxes are derived from ice cores by multiplying measured sulfate concentrations by the annual ice accumulation rate. To derive the volcanic sulfate deposition flux contribution the natural sulfate background level (e.g. due to marine biogenic sulfur emissions) is calculated in each ice core (the non-volcanic contribution) and a threshold flux value is chosen, above which sulfate is assumed to be of volcanic origin. The ice core-derived volcanic sulfate deposition flux is then calculated as the difference between a year with the volcanic contribution and the mean of the non-volcanic years, and the resulting reported volcanic sulfate deposition flux is the sum of the fluxes in these perturbed years (Ferris et al., 2011; Cole-Dai et al., 2013; Sigl et al., 2013). Our comparable model-simulated volcanic deposition flux is calculated as the sum of the sulfate deposition anomaly (perturbed run minus control run) over the duration of the deposition signal (~2-4 years). For SOCOL, which has a sectional aerosol scheme, diagnostics are available for the wet and dry components of the sulfate deposition. For modal models, each of these components is further split into the contribution from each aerosol size mode simulated in the models (nucleation, Aitken, accumulation, coarse). The sulfate deposition flux is calculated (comparable to the ice core derived values) as the sum of all of these wet and dry components with a composition of SO_4^{2-} only. In the following sections, we define 'total deposition' as referring to the sum of wet and dry deposition fluxes. We define 'volcanic sulfate deposition' to specify the sulfate deposition flux anomaly due to the eruption of Mt. Tambora, and use 'cumulative deposited sulfate' to specify the time-integrated volcanic sulfate deposition fluxes.

To compare the model-simulated results with ice core values, we calculate two statistical metrics; the Normalized Mean Bias (NMB) and correlation coefficient (r). NMB is defined by:

$$NMB = \frac{\sum_{i=1}^{N}(M_i - O_i)}{\sum_{i=1}^{N}(O_i)},$$
(1)

where O_i is the ice core derived sulfate deposition and M_i is the simulated sulfate deposition in the model grid box containing the ice core. N is the number of ice core records. For both NMB and r, each ice core is given equal weighting. We define a high correlation as $r > 0.7$ and low correlation as $r < 0.3$.

3 Results

3.1 Pre-industrial background sulfate deposition

Figure 1 shows the annual mean sulfate deposition fluxes in the pre-industrial control simulations (no Tambora) for each model. Areas of high background sulfate deposition fluxes are found in close proximity to sulfur emission sources such

5 as continuously degassing volcanoes (e.g. in South America and Indonesia) and along and near mid-latitude storm tracks ($30°$–$60°$) where aerosol is removed effectively by precipitation. Continuously degassing volcanic emissions are not included in MAECHAM. Sulfate deposition fluxes are higher over the oceans than over the land, mainly due to the emission of marine dimethyl sulfide (DMS). In general, the models have similar background sulfate deposition patterns, with the global mean total (wet + dry) sulfate deposition flux ranging from 78 kg SO_4 km^{-2} yr^{-1} (WACCM) to 173 kg SO_4 km^{-2} yr^{-1} (UKCA).

10 We find that the background pre-industrial global mean atmospheric sulfate burdens are similar between WACCM, MAECHAM and SOCOL, but ~3 times larger in UKCA (Fig. S1). Sulfur species included in each model are listed in Table S1. Although the models have similar background sulfate deposition patterns, the partitioning of wet and dry deposition fluxes differs markedly between the models (Table 3). MAECHAM deposits very little sulfate by dry processes compared to the other models with annual global-total dry deposited sulfate a factor of 40 less than the global-total wet deposited sulfate.

15 In SOCOL, dry deposited sulfate is approximately half the magnitude of wet deposited sulfate.

The sulfate deposited on Antarctica and Greenland is a very small fraction (less than 1%) of the sulfate deposited globally. In UKCA the sulfate deposited on the polar ice sheets is dominated by dry deposition, which is supported by observations (Legrand and Mayewski, 1997), especially in the Antarctic interior (Wolff, 2012). In contrast, in MAECHAM, SOCOL and WACCM the sulfate deposited on the polar ice sheets is dominated by wet deposition (i.e. through

20 precipitation), suggesting an issue with the deposition or precipitation representation. However, we find that the simulated total precipitation compares well between models both globally and over the poles (Fig. S2-S3) indicating the differences in wet and dry deposition partitioning are due to each model's deposition schemes.

The annual global-total deposition for both SO_2 and SO_4 is listed in Table 3 for each model. Included for reference is the equivalent preindustrial SO_X (SO_2 + SO_4) deposition from the multi-model mean of the Atmospheric Chemistry and

25 Climate Model Intercomparison Project (ACCMIP) (Lamarque et al., 2013, their Table S4a). The ACCMIP simulations were set up as time-slice experiments and the multi-model mean listed is an average of 6 models. UKCA compares well to the ACCMIP multi-model mean for dry SO_X, but the wet SO_X is 7 Tg higher and the SO_4 deposition (29 Tg) is also much higher when compared to the other models (13-19 Tg). MAECHAM has a similar total for wet SO_X compared to the ACCMIP multi-model mean, but dry deposition is a factor of 4 lower. WACCM has a similar total for wet SO_X deposition compared to

30 the ACCMIP multi-model mean but total SO_X is 5 Tg lower. SOCOL matches the ACCMIP multi-model mean for total SO_X.

Following the analysis of Lamarque et al. (2013) we have taken the average sulfate deposition fluxes from 1850 to 1860 (a non-volcanic period) in several ice cores from Antarctica and Greenland and compared the ice core fluxes to the

modelled polar sulfate deposition fluxes in the control simulations (Fig. 2). Ice core meta-data are included in the supplementary information (Table S2).

Overall, the four models simulate similar background sulfate deposition patterns and magnitudes and compare well to pre-industrial ice core sulfate fluxes. Compared to the ice cores, all models capture the lower sulfate deposition in the
5 interior of Antarctica and higher sulfate deposition toward the coast. However, model-simulated sulfate deposition in West Antarctica is higher; Antarctic NMB (Sec. 2, Eq. (1)) range from 1.3 (UKCA) to 2.9 (SOCOL). We find that the model-simulated Antarctic sulfate deposition and Antarctic ice core values are highly correlated for all models with r above 0.9 for all models (Fig. S4). Deposition over the Arctic is also well captured, with MAECHAM and WACCM slightly underestimating the sulfate deposition fluxes, both with NMB of -0.1. UKCA has a very small positive NMB of 0.009 but
10 SOCOL has the highest Arctic deposition with a NMB of 1.1. None of the models capture the low flux recorded in Alaska as also found by Lamarque et al. (2013).

The background polar sulfate deposition flux is highly correlated with the simulated mean polar precipitation for all models, which in general can explain the simulated deposition patterns. Correlation coefficients in the Arctic (60° to 90°) are between 0.8 (SOCOL, MAECHAM and UKCA) and 0.9 (WACCM). The correlation coefficients are slightly higher in the
15 Antarctic (-60° to -90°) with r = 0.9 for all models. We find that the Antarctic precipitation in each model matches measured accumulation rates in ice cores (Fig. S3), and with a high correlation with r values of 0.7 (SOCOL) to 0.9 (WACCM, UKCA). UKCA and WACCM have very small NMB of ~0.1. MAECHAM has a slightly higher NMB of 0.6 and SOCOL a NMB of 0.7. In the Arctic, the models also capture the precipitation reasonably well compared to the accumulation in the ice cores, with NMB of between 0.1 (UKCA) and 0.5 (WACCM) but low correlation coefficients (r lies between 0.1-0.2 for all
20 models). Thus, compared to the ice cores the models capture the magnitude and spatial pattern of the background polar precipitation. Overall, the magnitude of the deposited sulfate in WACCM, MAECHAM and SOCOL, where ice sheet deposition is dominated by wet deposition, is likely driven by the snow accumulation rates across the ice sheets, which is well represented by all models. In UKCA, although the polar deposition is correlated with the polar precipitation, the ice sheet deposition mostly occurs by dry deposition.

25 **3.2 1815 Mt. Tambora eruption sulfate deposition**

3.2.1 Inter-model comparison of sulfate deposition

Figure 3 shows the ensemble mean monthly volcanic sulfate deposition (left) and cumulative deposited sulfate (right) simulated by each model and highlights inter-model differences in the timing and spatial distribution of the deposited sulfate. Deposition occurs rapidly in MAECHAM with 35% of the global-total deposition occurring in 1815 and the majority
30 (60%) occurring in 1816. SOCOL simulates the sulfate deposition starting slightly later than in MAECHAM, with the majority of the deposition (75%) occurring in 1816. In contrast, only 9% of deposition in UKCA occurs in 1815, with 55% in 1816 and 29% in 1817. In WACCM the deposition occurs even later, with no deposition occurring in 1815. Instead, 32%

is deposited in 1816, 46% in 1817 and 17% in 1818. Deposition is longest in duration in WACCM and global-total sulfate deposition remains elevated at the end of the simulation (Fig. 4). In MAECHAM deposition returns to near background levels by ~30 months after the eruption and ~40 months for UKCA and SOCOL. We find individual ensemble members are similar for each model and the ensemble spread in the global-total volcanic sulfate deposition over time is small, as shown in Fig. 4.

In UKCA and WACCM most of the volcanic sulfate is deposited at mid-latitudes (30-60º). This contrasts with MAECHAM, where the deposition is globally more uniform, with greater deposition in the polar regions, and high deposited sulfate exceeding 360 kg SO_4 km^{-2} over West Antarctica, which is completely absent in the other models. In SOCOL, deposition is greatest in the Southern Hemisphere mid-latitudes.

The models vary in the simulated relative contribution of wet deposition of sulfate and dry deposition of sulfate to the global-total cumulative deposited sulfate (Table 4), although the global-total is always dominated by wet deposition, as was also the case with the background sulfate deposition (Fig. 1, Table 3). Dry deposited sulfate in MAECHAM is a factor 15 lower than the dry deposited sulfate simulated by UKCA and WACCM. SOCOL also simulates fairly low dry deposited sulfate (0.8 Tg S).

The temporal and spatial evolution of the volcanic sulfate deposition ultimately reflects the evolution of the atmospheric volcanic sulfate burdens and the precipitation in each model. Figure 5 shows the zonal mean monthly-mean and global-total monthly-mean atmospheric volcanic sulfate burdens for each model. MAECHAM has the fastest conversion of SO_2 to sulfate aerosol, with the global peak sulfate burden occurring only 4 months after the eruption (Fig. 5b). UKCA and SOCOL are next with the peak global sulfate burden occurring 6-7 months after the eruption, but the global burden in SOCOL decays a lot quicker than in UKCA. The global burden in WACCM peaks 12 months after the eruption and remains elevated until the end of the simulation and hence deposition in WACCM is longer-lived. In all models there is stronger transport of the sulfate aerosol to the Southern Hemisphere compared to the Northern Hemisphere (Fig. 5a) likely due to the Brewer Dobson Circulation, which is stronger in the winter hemisphere.

3.2.2 Multi-model comparison to ice core records

Although all four models simulated similar background pre-industrial (no Tambora) polar sulfate deposition (Fig. 2), the simulated polar volcanic sulfate deposition varies both spatially and in magnitude between the models. Figure 6 shows the simulated cumulative deposited sulfate for each model compared to the cumulative deposited sulfate measured in ice cores from Greenland and Antarctica for the 1815 Mt. Tambora eruption.

In general, the ice cores from Antarctica show lower volcanic sulfate deposition in East Antarctica and higher deposition over the Antarctic Peninsula, with deposited sulfate ranging from 12.7 kg SO_4 km^{-2} (East Antarctica, core NUS07-7) to 133 kg SO_4 km^{-2} (Antarctic Peninsula, core Siple). In Greenland the ice core estimates range from 25 kg SO_4 km^{-2} (B20) to 85.4 kg SO_4 km^{-2} (D3).

We find MAECHAM and SOCOL simulate too much deposited sulfate on Antarctica and Greenland compared to the ice cores records (also seen in Toohey et al., 2013), whereas UKCA and WACCM simulate deposited sulfate much closer to the ice core values (Fig. 6). For Antarctica the NMB are 3.9 for MAECHAM, 2.1 for SOCOL, -0.5 for WACCM and -0.7 for UKCA. For Greenland the biases are slightly lower: 2.6 for MAECHAM, 1.3 for SOCOL, 0.1 for WACCM and

5   -0.5 for UKCA. However, although MAECHAM is the model with the highest bias between the simulated cumulative deposited sulfate and ice core values, we find that the simulated Antarctic cumulative deposited sulfate in MAECHAM is highly spatially correlated with the ice core values ($r = 0.8$) and Greenland deposition is moderately correlated ($r = 0.6$). Hence MAECHAM captures the spatial pattern of the deposited sulfate, especially in Antarctica, with greater deposition on the Antarctic Peninsula and lower deposition in East Antarctica, but the magnitude of the deposition is a factor ~3.7 too

10 large. Figure 7 shows the ice core values versus the model-simulated cumulative deposited sulfate. Correlation coefficients are less than ~0.5 for all models except MAECHAM, although these models have lower mean biases. A figure where the simulated deposition in MAECHAM has been reduced by a factor of 3 to illustrate the well-captured spatial pattern of deposition is included in the supplementary information, Fig. S5 (SOCOL is also included in this figure). Both UKCA and WACCM, which are the higher resolution models, simulate a strong gradient in deposition between the low deposition over

15 land and high deposition over sea and although they match the magnitude of the cumulative deposited sulfate more closely on the ice sheets than SOCOL and MAECHAM, they fail to produce the high values of cumulative deposited sulfate on the Antarctic Peninsula. Although cumulative deposited sulfate in SOCOL is not highly correlated with the ice core values across the whole of the Antarctic ice sheet, this model does simulate higher cumulative deposited sulfate over the Antarctic Peninsula. The polar deposition in UKCA and WACCM more closely follows the models' precipitation field, with

20 correlation coefficients between the polar (60º-90º) precipitation (averaged over the four years after the eruption) and polar cumulative deposited sulfate (in the four years after the eruption) of 0.7 and 0.9 respectively. Polar correlation coefficients for SOCOL are very low at 0.2 in the Arctic and 0.1 in the Antarctic and for MAECHAM are 0.6 in the Arctic and 0.4 in the Antarctic. Figure 8 shows the zonal mean precipitation and zonal mean cumulative deposited sulfate in each model. The precipitation in the models is very similar, suggesting that the differences in model-simulated volcanic sulfate deposition

25 arise from differences in the transport of the sulfate aerosol to the polar regions and/or the deposition schemes themselves. The ice sheet sulfate deposition in UKCA remains dominated by dry deposition.

Figure 9 shows the simulated area-mean volcanic sulfate deposition to the Antarctic and Greenland ice sheets over time for each model. Included for comparison are two of the highest resolved and most precisely dated ice cores (D4: McConnell et al., 2007; DIV: Sigl et al., 2014). We find that deposition to both ice sheets peaks first in MAECHAM,

30 followed by SOCOL, then UKCA and WACCM. The main phase of deposition recorded in the two ice cores falls in time between that simulated by MAECHAM and the other models. Compared to DIV and D4, the deposition to the ice sheets in MAECHAM is too quick, but too slow in WACCM and UKCA, although the timing is still relatively well captured for all models. The onset and duration of deposition to the ice sheets simulated by SOCOL is most comparable to the two ice cores, but simulated deposition is too large (see Fig. 6) and does not exhibit the variability in time apparent in the two ice core

deposition time series. WACCM simulates the greatest variability in ice sheet deposition over time, with several peaks and troughs in the deposition time series. The ice sheet deposition simulated in WACCM is longer in duration than measured in the two ice cores (see also Fig. 10 for further time series of the model-simulated ice sheet deposition).

3.3 Relationship between hemispheric atmospheric sulfate burdens and sulfate deposited on ice sheets

5   In order to derive the relationships between the hemispheric atmospheric sulfate burdens and the sulfate deposited on the ice sheets, we calculate the cumulative mean sulfate deposited on Antarctica and Greenland, calculated as the area-weighted mean deposited sulfate on each ice sheet once a land-sea mask has been applied. We calculate the ratio between Antarctica and Greenland deposited sulfate and the ratio between the Southern Hemisphere (SH) peak atmospheric sulfate burden and Northern Hemisphere (NH) peak atmospheric sulfate burden. Next we calculate the ratio between the

10   hemispheric peak atmospheric sulfate burdens [Tg SO_4] (representing the total amount of sulfate aerosol that has formed) and the average amount of sulfate deposited on each ice sheet [kg SO_4 km^{-2}] for each of the models. We refer to this ratio as the Burden-To-Deposition factor (BTD), which is equivalent to the scaling factors derived by Gao et al. (2007).

In all models the SH peak atmospheric sulfate burden is greater than the NH atmospheric sulfate burden (Table 5) due to seasonal preferential transport of the sulfate aerosol to the SH in all simulations (Fig. 5a). Ratios between the SH and

15   NH burdens are between 1.4 and 1.9. However, despite the larger SH burden, only MAECHAM and SOCOL simulate greater Antarctica mean deposited sulfate than in Greenland. WACCM has the smallest deposition ratio (0.3) with mean Greenland deposited sulfate of 109 kg SO_4 km^{-2} compared to 36 kg SO_4 km^{-2} in Antarctica. MAECHAM and SOCOL have the closest deposition ratio to that derived by Sigl et al. (2015), but with mean deposited sulfate ~3-6 times larger than the ice core estimates. Conversely, and as simulated in UKCA and WACCM, the mean deposited sulfate deduced by Gao et al.

20   (2007) showed slightly more mean deposited sulfate on Greenland relative to Antarctica, with a ratio of 0.9, although this ratio is still much larger than in UKCA and WACCM. In contrast to MAECHAM and SOCOL, where the deposition ratio mirrors the hemispheric split of the sulfate aerosol, deposition ratios for both UKCA and WACCM are dissimilar to the ratio of the hemispheric peak burdens.

To explore possible mechanisms for the differences between the hemispheric atmospheric sulfate burden ratios and

25   deposition ratios, we have examined the temporal evolution of the ice sheet deposition compared with the sulfate burdens (Fig. 10). In MAECHAM the NH sulfate burden peaks only 2 months after the eruption and the SH burden peaks 4 months after the eruption. The ice sheet deposition follows suit with the majority of deposition to Greenland occurring 8 months after the eruption and peak deposition to Antarctica occurring 14 months after the eruption. However, in the other models the SH burden peaks before the NH peak burden. The SH burden is greatest between 5-7 months after the eruption in these

30   models and the NH burden peaks between 10-12 months after the eruption. In contrast to MAECHAM, there are no clear separate peaks between the deposition to each ice sheet. In SOCOL, both the majority of Greenland and Antarctic deposition occurs between 10-20 months after the eruption. In UKCA and WACCM the main phase of deposition is longer lived and occurs between 10-30 months after the eruption and there is more variability in the deposition timeseries compared to

MAECHAM and SOCOL. Overall, decay of the atmospheric sulfate burden and deposition to the ice sheets in MAECHAM is rapid, occurring within the first 20 months after the eruption, suggesting a fast transport of sulfate aerosol to the poles. We find that in the first ~8 months after the eruption the sulfate burden in UKCA and WACCM is restricted between ~60 °S and ~40 °N (Fig. 5a), with strong gradients in sulfate burden across the SH polar vortex and NH subtropical edge, whereas more

5   sulfate is transported to the poles in MAECHAM and SOCOL.

The strength of the background climatological winds differs slightly in each model, with the strongest polar jets simulated in WACCM, and weakest in MAECHAM (maximum zonal mean climatological zonal winds are 52 m s^{-1} in WACCM and 32 m s^{-1} in MAECHAM (Fig. S6)). All models simulate a strengthening in the NH and SH polar zonal winds in the first year after the eruption; WACCM simulates the largest zonal mean anomalies and MAECHAM the weakest. All

10   models simulate a clear strengthening of the southern polar vortex ~3-8 months after the eruption (defined here as the zonal mean zonal wind at the grid boxes closest to 60°S and 10 hPa), with a peak anomaly of 30 m s^{-1} simulated in WACCM (Fig. S7). Figure 11 shows the zonal mean zonal wind averaged over the first year after the eruption in each model. Peak zonal mean SH polar zonal wind is 58 m s^{-1} in WACCM, 45 m s^{-1} in UKCA, 44 m s^{-1} in SOCOL and 38 m s^{-1} in MAECHAM.

The polar vortex inhibits the transport of stratospheric aerosol to the poles (e.g. Schoeberl & Hartmann, 1991), with

15   the stronger polar vortex in WACCM likely restricting some of the sulfate deposition in Antarctica compared to MAECHAM, which simulates the weakest winds. Differences in the polar vortex strength in each model may therefore contribute to the differences in simulated polar sulfate deposition but more work is needed to assess the dynamical response to the eruption of Tambora in these models. This remains beyond the scope of the current paper.

Next, we examine the range in BTD factors across the models. BTD factors are important for estimating the

20   hemispheric atmospheric sulfate burden and subsequently estimating the forcing of historical volcanic eruptions based on ice core sulfate deposition records. We calculate the BTD factors for both NH (NH_BTD) and SH (SH_BTD), defined as the ratio between the hemispheric peak atmospheric sulfate burden [Tg SO$_4$] and the mean ice sheet deposited sulfate [kg SO$_4$ km^{-2}] (Table 6). BTD factors for MAECHAM are the same for both the NH and SH, as in Gao et al. (2007), but a factor 5 lower than Gao et al. (2007). WACCM, SOCOL and UKCA simulate smaller NH_BTD than SH_BTD, but these factors are

25   different in each model, with the NH_ BTD ranging from 0.27 *10^9 km^{-2} (SOCOL) to 0.97 *10^9 km^{-2} (UKCA) and the SH_BTD from 0.33 *10^9 km^{-2} (SOCOL) to 2.91 *10^9 km^{-2} (UKCA). All models simulate a NH_BTD less than 1 *10^9 km^{-2}, but SH_BTD are less than 1 *10^9 km^{-2} for only MAECHAM and SOCOL due to the much larger Antarctic deposition in these models compared to UKCA and WACCM. The multi-model mean NH_BTD factor is 0.44 *10^9 km^{-2} and multi-model mean SH_BTD factor is 1.26 *10^9 km^{-2}. These factors are ~40% different to the mean factors derived by Gao et al. (2007),

30   which were calculated from the observed relationship between the atmospheric burden and deposition of radioactive material after nuclear bomb tests. We also find variability in the BTD factors across the individual ensemble members for each model arising due to internal variability, but ensemble spread is smaller than the inter-model spread.

We also test the sensitivity of the derived model BTD factors in Table 6 if we take polar deposition (60°-90°N/S) as opposed to ice sheet deposition, given that both UKCA and WACCM simulate strong gradients in cumulative deposited

sulfate across the land-sea boundary (Fig. 6). We find that the BTD factors remain similar for SOCOL and MAECHAM, but are reduced by up to a factor of 3 in UKCA and WACCM due to the mean polar cumulative deposited sulfate being greater than the mean ice sheet cumulative deposited sulfate (Table S4). This reduces the spread in the BTD factors between the models and results in a reduction of the multi-model mean NH_BTD factor from $0.44 *10^9$ km^{-2} to $0.27 *10^9$ km^{-2} and the

5   SH_BTD from $1.26 *10^9$ km^{-2} to $0.53 *10^9$ km^{-2}.

4 Discussion

4.1 Differences in deposited sulfate

The spatial pattern and magnitude of deposited sulfate depends on the sources of atmospheric SO_2, the transport and mixing of the sulfate aerosol formed throughout the stratosphere and across the tropopause as well as its deposition by either

10   precipitation or gravitational sedimentation (e.g. Hamill et al., 1997; Kremser et al., 2016). In the pre-industrial background state (no Tambora) (Fig. 1), all four models examined simulate similar patterns of sulfate deposition, with more sulfate deposited at the mid-latitudes and near SO_2 sources such as continuously degassing volcanoes. In the polar regions, the models also simulated similar sulfate deposition and matched the magnitude and spatial pattern recorded in ice cores (Fig. 2). This indicates that the models may be accurately simulating aspects of the formation and transport of background sulfate

15   aerosol and subsequent deposition processes, albeit with differences in the ratio of wet and dry deposition. UKCA was the only model to simulate a greater proportion of background deposition to the ice sheets occurring by dry processes. We find that all models simulate similar precipitation, which compares well to the annual snow accumulation recorded in ice cores and that the polar sulfate deposition is highly correlated with the polar precipitation.

However, under the volcanically-perturbed conditions (with Tambora), the simulated volcanic sulfate deposition

20   differs between all models. Compared to ice core records of cumulative deposited sulfate for 1815 Mt. Tambora, MAECHAM and SOCOL simulate too high deposition to polar regions and UKCA and WACCM simulate too little deposition to polar regions. In UKCA and WACCM, the polar cumulative deposited sulfate more closely follows the spatial pattern of precipitation, although on the actual ice sheets, deposition in UKCA is dominated by dry deposition. In MAECHAM and SOCOL the polar cumulative deposited sulfate is more enhanced compared to the precipitation (Fig. 8).

25   However, MAECHAM simulates the best spatial correlations with the ice cores, further indicating that precipitation is not the sole driver of the spatial variability of deposited volcanic sulfate. As these models were able to match the ice core fluxes in the background state, it stands that in the Tambora case, the poleward transport of aerosol in UKCA and WACCM is too weak or mid-latitude deposition is too strong. In MAECHAM and SOCOL the polar volcanic deposition is too strong likely because of a high bias in poleward aerosol transport (Toohey et al., 2013). MAECHAM and SOCOL also have the lowest

30   resolution of the four models (Table 1), which may contribute to the high deposition bias since stratospheric circulation and cross-tropopause transport is better represented in higher resolution models (e.g. Toohey et al., 2013). Gao et al. (2007), using the GISS ModelE, found that simulated deposited sulfate over the poles after the eruption of Mt. Tambora was a factor

of two too large, but that the spatial pattern of deposition recorded in ice cores was well captured. GISS ModelE had a much lower resolution than the models used here (4° x 5°) and a simplified scheme for stratospheric aerosol microphysics. It is also likely that smoother topography in these lower resolution models will influence the spatial pattern of deposition.

The timing and duration of sulfate deposition mirrors that of the atmospheric sulfate burdens. In MAECHAM the
5 atmospheric sulfate burden peaks sooner and decays more quickly than in the other models, and the ice sheet deposition occurs more rapidly (within the first 2 years after the eruption). The atmospheric sulfate burden in WACCM is still elevated 5 years after the eruption, and hence the deposition signal is also longer-lived; deposition still occurs in 1819, four years after the eruption (Fig. 4).

The size of the volcanic sulfate aerosol particles will impact the simulated sulfate deposition by affecting the
10 particle sedimentation rates. Most of the volcanic sulfate aerosol resides in the accumulation mode for UKCA and MAECHAM, but in the larger coarse mode for WACCM, and WACCM has the strongest mid-latitude volcanic deposition where cross-tropopause transport occurs (Fig. 3). Furthermore, MAECHAM is the only model that has prescribed OH as opposed to interactive OH. OH may become depleted in dense volcanic clouds by reaction with SO_2, affecting the rate of sulfate aerosol formation (Bekki, 1995). The lack of interactive OH in MAECHAM should result in more rapid oxidation of
15 the volcanic SO_2 into sulfate aerosol compared to the other models. Although it is beyond the scope of this paper to address all of the model differences in sulfur chemistry and the formation of the volcanic aerosol, the chemistry and aerosol microphysics are ultimately important factors affecting deposition patterns. Further work on the aerosol size and growth processes will allow a more detailed understanding of some of the model differences identified here.

The direction and strength of the stratospheric winds impacts the transport of sulfate aerosol and hence where it is
20 deposited. UKCA, WACCM and SOCOL have similarly defined QBOs with downward propagating easterly and westerly winds, with the eruption simulated in the easterly phase. MAECHAM does not include a QBO and although stratospheric winds were easterly in the MAECHAM simulations, we find that these winds are ~20 m s^{-1} weaker than the easterly phase winds in the other models (Fig. S8). This may explain the quicker transport and subsequent deposition to the poles in the MAECHAM simulations as strong easterly winds restrict the meridional movement of aerosol (Trepte and Hitchman, 1992).
25 In addition to mid-latitude tropopause folds, a further location of cross-tropopause transport of sulfate aerosol is the polar winter vortex (e.g. SPARC, 2006; Kremser et al., 2016). The polar vortex inhibits poleward transport, and it has been suggested that variations in the strength of polar vortex may modulate volcanic aerosol transport and deposition to polar ice sheets (Toohey et al, 2013). Inter-model differences in polar vortex strength may therefore contribute to differences in polar sulfate deposition. Following this hypothesis, the strong SH polar vortex simulated by WACCM may contribute to the large
30 SH_BTD values for this model, and likewise, the relatively weaker polar vortex in MAECHAM may contribute to small SH_BTD values. On the other hand, UKCA simulates average polar vortex winds, but the largest SH_BTD values. Therefore, it appears to be a combination of factors that drive the inter-model differences in simulated polar volcanic sulfate deposition.

4.2 Implications for the relationship between hemispheric atmospheric sulfate burdens and sulfate deposited on ice sheets

Using just four global aerosol models, we find large differences in the mean deposited sulfate on Antarctica and Greenland. The multi-model mean BTD factor, which relates the atmospheric sulfate burden to the deposition at the ice sheets, differed on average by ~40% from the estimates by Gao et al. (2007), although the Gao et al. (2007) estimates are within or close to the multi-model spread. We find that the multi-model spread in BTD factors is reduced when we take a polar cap average of deposition as opposed to the average ice sheet deposition because simulated deposition is more similar amongst the models when a greater area average is considered. Due to the large gradient between land and sea deposition simulated in WACCM and UKCA, mean polar deposition does not represent the mean ice sheet deposition and BTD factors are therefore sensitive to the areas chosen to represent the polar/ice sheet deposition. This makes it difficult to estimate accurately the relationship between ice sheet deposition and sulfate aerosol loading in the models. We highlight this to emphasize caution when determining BTD factors in future modelling studies. Furthermore, although these simulations aimed to follow a common protocol, the injection setup did differ between models due to differences in the ways modelling groups interpret and simulate a volcanic injection (Table 2). This is a common problem in multi-model comparisons and makes it more difficult to isolate and attribute model differences.

We did not expect the models to be able to simulate the exact deposition at each ice core location given the large natural variability in local weather and snow patterns, which will be different in the models, uncertainties in estimating ice core volcanic sulfate deposition and in model inputs (e.g. magnitude and altitude of the volcanic sulfur emission), and fundamentally, that in the real world there was only one realization of weather. Even if the models were perfect, they could not predict the actual deposition pattern as they could not simulate the actual weather that occurred. Regarding the model inputs, there are no good observations of the injection altitude of SO_2 from the 1815 Mt. Tambora eruption, and often simulations are initiated with SO_2 injected at heights lower than the estimated injection altitude, to account for self-lofting as the aerosol forms. Here, simulations followed the common protocol but it may be that to better simulate the eruption of Mt. Tambora, sensitivity to injection height should be explored. Models may also contain inaccuracies due to uncertain physical representations and coarse resolution, and several ice core locations will be represented by the same model grid box. The differing resolutions between the models also means that the number of grid boxes and area that defines each ice sheet differs slightly between the models. Sulfate deposition fluxes have a large spatial variability due to differences in precipitation, the local synoptic conditions at the time of deposition, and post-deposition movement through wind (Fisher et al., 1985; Robock and Free, 1995; Wolff et al., 2005). Deposition fluxes can vary by orders of magnitude, even between ice cores that are located close to each other. For example, in a very low accumulation site in Antarctica (Dome C), Gautier et al. (2016) found that in five cores drilled 1 m apart, two cores missed the Tambora sulfate flux signal completely, which they attributed to snow drift and surface roughness. They reported that the mean flux between these five cores is uncertain by ~30%, highlighting the uncertainties in sulfate fluxes reported from single cores at such a low-accumulation site. This

appears to be an extreme case, however, and the 1815 Mt. Tambora signal is clearly identifiable in all other Antarctic ice cores (Sigl et al., 2014).

Furthermore, the phase of the QBO at the time of the eruption is unknown, and here we have only used simulations where the SO_2 is emitted during the easterly phase. Toohey et al. (2013) also found that deposition to the poles varied as a function of SO_2 injection magnitude and season, and their simulations of a Tambora-like eruption showed greater deposition to Greenland than Antarctica. However, the volcanic eruptions in Toohey et al. (2013) were simulated in January and July, located at 15°N, which may explain the bias towards Greenland deposition. Further work is required on the influence of the QBO phase and injection height on the Antarctic and Greenland deposition efficiency.

Our multi-model mean NH_BTD factor is ~60% lower than previously derived (Gao et al., 2007), which if used to estimate the NH atmospheric sulfate burden of other historic tropical eruptions from their mean Greenland deposited sulfate, would result in lower burdens, and likely less volcanic cooling. Model-simulated NH cooling following large-magnitude volcanic eruptions has been overestimated in the past (e.g. Stoffel et al., 2015; Zanchettin et al., 2016). However, our multi-model mean SH_BTD factor is ~20% greater than Gao et al. (2007), which would result in a larger SH sulfate burden estimate. Applying our BTD factors (NH: 0.44 and SH: 1.26) to the mean Greenland and Antarctic deposited sulfate from the 1257 Samalas eruption (90 kg km^{-2} and 73 kg km^{-2}, respectively (Sigl et al., 2015)), results in a considerable hemispheric asymmetry in the estimated sulfate burdens. We calculate a SH burden ~2 times the NH burden, despite the eruption occurring in the tropics. This could result in further differences in aerosol optical depth and volcanic aerosol radiative forcing, and hemispheric asymmetry in atmospheric sulfate burdens has been shown to shift the inter-tropical convergence zone leading to precipitation anomalies (e.g. Haywood et al., 2013). However, this asymmetry seems unlikely, given that cooling in the SH after large tropical eruptions appears limited in proxy records (Neukom et al., 2014).

5 Conclusions

We have analysed the volcanic sulfate deposition in model simulations of the 1815 eruption of Mt. Tambora using four state-of-the-art global aerosol models (WACCM, MAECHAM, SOCOL and UKCA) and compared the simulated deposited sulfate to a comprehensive array of ice core records. We have investigated the sulfate deposition to the poles under both pre-industrial background conditions (no Tambora) and volcanically perturbed (with Tambora) conditions. Although all models simulated similar background sulfate deposition fluxes, which compare well to polar ice core records, the models differ substantially in their simulation of the Mt. Tambora volcanic sulfate deposition. WACCM and UKCA simulate comparable deposition patterns but underestimate the volcanic sulfate deposited on the ice sheets, with strong gradients in the deposited sulfate between land and sea. MAECHAM simulates a spatial pattern of deposited sulfate similar to ice cores, but the magnitude is ~3 times too large. Ice sheet deposited sulfate in SOCOL is also too large compared to ice cores.

The models simulate similar precipitation rates and patterns, which compare well to the annual snow accumulation recorded in ice cores. Hence, differences in the model-simulated volcanic sulfate deposition likely arise due to differences in

the simulated atmospheric sulfate aerosol burdens and aerosol transport. In WACCM and UKCA the volcanic sulfate deposition is more related to the precipitation fields, with more sulfate deposited at the mid-latitude storm belts, than in MAECHAM and SOCOL. In MAECHAM and SOCOL, enhanced transport of sulfate aerosol to the poles dictates the resulting high ice sheet sulfate deposition. We suggest that a combination of differences in model resolution, modelled

5   stratospheric winds and deposition schemes in each model have all contributed to the resulting differences in volcanic sulfate deposition.

We have calculated Burden-To-Deposition (BTD) factors between the mean deposited sulfate on each ice sheet and the corresponding hemispheric peak atmospheric sulfate burden for the Mt. Tambora simulations (Table 6). The BTD factors differ by up to a factor of 15 between the models. The multi-model mean BTD factors differ on average by ~40% to BTD

10   factors currently used to deduce historical volcanic forcing (e.g. Gao et al., 2007; 2008; Sigl et al., 2015). Our derived BTD factors highlight uncertainties in the relationship between atmospheric sulfate burden and ice sheet deposited sulfate for this eruption.

We find very large differences in model-simulated volcanic sulfate deposition from the 1815 eruption of Mt. Tambora and in the relationship between atmospheric sulfate burden and ice sheet deposited sulfate. Given that GISS

15   ModelE (Gao et al., 2007) did as good a job at simulating the deposited sulfate from this eruption as these newer, higher-resolution models, which also have more sophisticated treatments of gas-to-aerosol conversion, and the fact that the four models used here simulate very different sulfate deposition, it remains an open research question as to the optimal model configuration for this problem. A detailed analysis of the differences in sulfur chemistry and the aerosol formation and transport in each model will further aid in the interpretation of these results. Using idealized prescribed aerosol forcings such

20   as Easy Volcanic Aerosol (Toohey et al., 2016) in future VolMIP experiments, will provide the opportunity to better understand model diversity and to advance our understanding of the climate response to large volcanic eruptions. Simulations of other large-magnitude volcanic eruptions will also enable the calculation of additional multi-model BTD factors, which will aid in the calculation of historic volcanic forcing.

25   **Competing interests.** The authors declare that they have no conflict of interest.

Special issue statement. This article is part of the multi-journal special issue "The Model Intercomparison Project on the climatic response to Volcanic forcing (VolMIP)". It does not belong to a conference.

30   **Acknowledgments.** Lauren Marshall is supported by the Natural Environment Research Council (NERC), UK through the Leeds-York NERC Doctoral Training Partnership. Anja Schmidt was funded by an Academic Research Fellowship from the University of Leeds. Alan Robock is supported by U.S. National Science Foundation grant AGS-1430051. Claudia Timmreck received funding from the German Federal Ministry of Education and Research (BMBF), research program

"MiKliP"(FKZ: 01LP1517B). Ulrike Niemeier, Claudia Timmreck and Slimane Bekki acknowledge support received funding from the European Union FP7 project "STRATOCLIM" (FP7-ENV.2013.6.1-2; Project 603557). MAECHAM simulations were performed at the German climate Computer Centre (DKRZ). Fiona Tummon was funded by Swiss National Science Foundation grant 20F121_138017. This study benefited from the support of the Labex L-IPSL which is

5   funded by the ANR (Grant #ANR-10-LABX-0018). Matthew Toohey acknowledges support by the Deutsche Forschungsgemeinschaft (DFG) in the framework of the priority programme "Antarctic Research with comparative investigations in Arctic ice areas" through grant TO 967/1-1. The National Center for Atmospheric Research is funded by the National Science Foundation. Eugene Rozanov and Timofei Sukhodolov acknowledge support from the Swiss National Science Foundation under grant 200021_169241 (VEC).

References

Bekki, S.: Oxidation of volcanic SO2: A sink for stratospheric OH and H2O, Geophys. Res. Lett., 22(8), 913–916, doi:10.1029/95GL00534, 1995.

Clausen, H. B., and Hammer, C. U.: The laki and tambora eruptions as revealed in greenland ice cores from 11 locations, Ann. Glaciol., 10, 16-22, 1988.

Cole-Dai, J., Mosley-Thompson, E., and Thompson, L. G.: Annually resolved southern hemisphere volcanic history from two Antarctic ice cores, J. Geophys. Res., 102(D14), 16761–16771, doi:10.1029/97JD01394, 1997.

Cole-Dai, J., Mosley-Thompson, E., Wight, S. P., and Thompson, L. G.: A 4100-year record of explosive volcanism from an East Antarctica ice core, J. Geophys. Res., 105(D19), 24431–24441, doi:10.1029/2000JD900254, 2000.

Cole-Dai, J., Ferris, D. G., Lanciki, A. L., Savarino, J., Thiemens, M. H., and McConnell, J. R.: Two likely stratospheric volcanic eruptions in the 1450s C.E. found in a bipolar, subannually dated 800 year ice core record, J. Geophys. Res., 118(14), 7459–7466, doi:10.1002/jgrd.50587, 2013.

Crowley, T. J.: Causes of Climate Change Over the Past 1000 Years, Science, 289(5477), 270-277, 2000.

Crowley, T. J. and Unterman, M. B.: Technical details concerning development of a 1200 yr proxy index for global volcanism, Earth Syst. Sci. Data, 5, 187–197, doi:10.5194/essd-5-187-2013, 2013.

Dhomse, S. S., Emmerson, K. M., Mann, G. W., Bellouin, N., Carslaw, K. S., Chipperfield, M. P., Hommel, R., Abraham, N. L., Telford, P., Braesicke, P., Dalvi, M., Johnson, C. E., O'Connor, F., Morgenstern, O., Pyle, J. A., Deshler, T., Zawodny, J. M., and Thomason, L. W.: Aerosol microphysics simulations of the Mt. Pinatubo eruption with the UM-UKCA composition-climate model, Atmos. Chem. Phys., 14, 11221–11246, doi:10.5194/acp-14-11221-2014, 2014.

Eyring, V., Bony, S., Meehl, G. A., Senior, C. A., Stevens, B., Stouffer, R. J., and Taylor, K. E.: Overview of the Coupled Model Intercomparison Project Phase 6 (CMIP6) experimental design and organization, Geosci. Model Dev., 9, 1937–1958, doi:10.5194/gmd-9-1937-2016, 2016.

Ferris, D. G., Cole-Dai, J., Reyes, A. R., and Budner, D. M.: South Pole ice core record of explosive volcanic eruptions in the first and second millennia A.D. and evidence of a large eruption in the tropics around 535 A.D., J. Geophys. Res., 116, D17308, doi:10.1029/2011JD015916, 2011.

Fisher, D. A., Reeh, N., and Clausen, H. B.: Stratigraphic noise in time series derived from ice cores, Ann. Glaciol., 7, 76–

83, 1985.

Gao, C., Robock, A., Self, S., Witter, J.B., Steffenson, J.P., Clausen, H.B., Siggaard- Andersen, M.L., Johnsen, S.,
   Mayewski, P.A. and Ammann, C.: The 1452 or 1453 A.D. Kuwae eruption signal derived from multiple ice core
   records: Greatest volcanic sulfate event of the past 700 years, J. Geophys. Res., 111, D12107,
5   doi:10.1029/2005JD006710, 2006.

Gao, C., Oman, L., Robock, A., and Stenchikov, G. L.: Atmospheric volcanic loading derived from bipolar ice cores:
   Accounting for the spatial distribution of volcanic deposition, J. Geophys. Res, 112, D09109,
   doi:10.1029/2006JD007461, 2007.

Gao, C., Robock, A., and Ammann, C.: Volcanic forcing of climate over the past 1500 years: an improved ice core-based
10   index for climate models, J. Geophys. Res., 113, D23111, doi:10.1029/2008JD010239, 2008.

Gautier, E., Savarino, J., Erbland, J., Lanciki, A., and Possenti, P.: Variability of sulfate signal in ice core records based on
   five replicate cores, Clim. Past, 12, 103–113, doi:10.5194/cp-12-103-2016, 2016.

Hamill, P., Jensen, E. J., Russell, P. B., and Bauman, J. J.: The Life Cycle of Stratospheric Aerosol Particles, Bulletin of the
   American Meteorological Society, 78(7), 1395–1410, 1997.

15   Haywood, J. M., Jones, A., Bellouin, N., and Stephenson, D.: Asymmetric forcing from stratospheric aerosols impacts
   Sahelian rainfall, Nat. Clim. Change, 3, 660–665, doi:10.1038/nclimate1857, 2013.

Herzog, M. and Graf, H.-F.: Applying the three-dimensional model ATHAM to volcanic plumes: dynamic of large co-
   ignimbrite eruptions and associated injection heights for volcanic gases, Geophys. Res. Lett., 37, L19807,
   doi:10.1029/2010GL044986, 2010.

20   Kremser, S., Thomason, L. W., Hobe, M., Hermann, M., Deshler, T., Timmreck, C., Toohey, M., Stenke, A., Schwarz, J. P.,
   Weigel, R., Fueglistaler, S., Prata, F. J., Vernier, J.-P., Schlager, H., Barnes, J. E., Antuña-Marrero, J.-C., Fairlie, D.,
   Palm, M., Mahieu, E., Notholt, J., Rex, M., Bingen, C., Vanhellemont, F., Bourassa, A., Plane, J. M. C., Klocke, D.,
   Carn, S. A., Clarisse, L., Trickl, T., Neely, R., James, A. D., Rieger, L., Wilson, J. C. and Meland, B.: Stratospheric
   aerosol–Observations, processes, and impact on climate, Rev. Geophys., 54(2), 278–335, doi:10.1002/2015RG000511,
25   2016.

Lamarque, J.-F., Dentener, F., McConnell, J., Ro, C.-U., Shaw, M., Vet, R., Bergmann, D., Cameron-Smith, P., Dalsoren, S.,
   Doherty, R., Faluvegi, G., Ghan, S. J., Josse, B., Lee, Y. H., MacKenzie, I. A., Plummer, D., Shindell, D. T., Skeie, R.
   B., Stevenson, D. S., Strode, S., Zeng, G., Curran, M., Dahl-Jensen, D., Das, S., Fritzsche, D., and Nolan, M.: Multi-

model mean nitrogen and sulfur deposition from the Atmospheric Chemistry and Climate Model Intercomparison Project (ACCMIP): evaluation of historical and projected future changes, Atmos. Chem. Phys., 13, 7997-8018, doi:10.5194/acp-13-7997-2013, 2013.

Langway, C. C., Osada, K., Clausen, H. B., Hammer, C. U., and Shoji, H.: A 10-century comparison of prominent bipolar volcanic events in ice cores, J. Geophys. Res., 100(D8), 16241–16247, doi:10.1029/95JD01175, 1995.

Legrand, M., & Mayewski, P.: Glaciochemistry of polar ice cores: A review, Rev. Geophys., 35(3), 219–243, doi:10.1029/96RG03527, 1997.

McCormick, M. P. and Veiga, R. E.: SAGE II measurements of early Pinatubo aerosols, Geophys. Res. Lett., 19, 155–158, doi:10.1029/91GL02790, 1992.

Mills, M. J., Schmidt, A., Easter, R., Solomon, S., Kinnison, D. E., Ghan, S. J., Neely III, R. R., Marsh, D. R., Conley, A., Bardeen, C. G., and Gettelman, A.: Global volcanic aerosol properties derived from emissions, 1990–2014, using CESM1(WACCM). J. Geophys. Res.-Atmos., 121, 2332–2348, doi:10.1002/2015JD024290, 2016.

Niemeier, U., Timmreck, C., Graf, H.-F., Kinne, S., Rast, S., and Self, S.: Initial fate of fine ash and sulfur from large volcanic eruptions, Atmos. Chem. Phys., 9, 9043–9057, doi:10.5194/acp- 9-9043-2009, 2009.

Oppenheimer, C.: Climatic, environmental and human consequences of the largest known historic eruption: Tambora volcano (Indonesia) 1815, Prog. Phys. Geog., 27, 230–259, 2003.

Pinto, J. P., Toon, O. B., and Turco, R. P.: Self-limiting physical and chemical effects in volcanic eruption clouds, J. Geophys. Res., 94, 11165–11174, doi:10.1029/JD094iD08p11165, 1989.

Raible, C. C., Brönnimann, S., Auchmann, R., Brohan, P., Frölicher, T. L., Graf, H.-F., Jones, P., Luterbacher, J., Muthers, S., Neukom, R., Robock, A., Self, S., Sudrajat, A., Timmreck, C., and Wegmann, M.: Tambora 1815 as a test case for high impact volcanic eruptions: Earth system effects, WIREs Clim Change, 7, 569–589, doi:10.1002/wcc.407, 2016.

Read, W. G., Froidevaux, L., and Waters, J. W.: Microwave limb sounder measurement of stratospheric SO_2 from the Mount Pinatubo volcano, Geophys. Res. Lett., 20, 1299–1302, doi:10.1029/93GL00831, 1993.

Robock, A.: Volcanic eruptions and climate, Rev. Geophys., 38(2), 191–219, 2000.

Robock, A., and Free, M. P.: Ice cores as an index of global volcanism from 1850 to the present, J. Geophys. Res., 100(D6), 11549-11567, doi:10.1029/95JD00825, 1995.

Schoeberl, M. R., and Hartmann, D. L.: The Dynamics of the Stratospheric Polar Vortex and Its Relation to Springtime Ozone Depletions, Science, 251(4989), 46–52, doi:10.1126/science.251.4989.46, 1991.

Self, S., Gertisser, R., Thordarson, T., Rampino, M. R., and Wolff, J. A.: Magma volume, volatile emissions, and stratospheric aerosols from the 1815 eruption of Tambora, Geophys. Res. Lett. 31, L20608, doi:10.1029/2004GL020925, 2004.

Sheng, J.-X., Weisenstein, D. K., Luo, B.-P., Rozanov, E., Stenke, A., Anet, J., Bingemer, H., and Peter, T.: Global atmospheric sulfur budget under volcanically quiescent conditions: aerosol– chemistry–climate model predictions and validation, J. Geophys. Res.-Atmos., 120, 256–276, doi:10.1002/2014JD021985, 2015.

Sigl, M., McConnell, J. R., Layman, L., Maselli, O., McGwire, K., Pasteris, D., Dahl-Jensen, D., Steffensen, J. P., Vinther, B., Edwards, R., Mulvaney, R. and Kipfstuhl, S.: A new bipolar ice core record of volcanism from WAIS Divide and NEEM and implications for climate forcing of the last 2000 years, J. Geophys. Res.-Atmos., 118(3), 1151–1169, doi: 10.1029/2012JD018603, 2013.

Sigl, M., Mcconnell, J. R., Toohey, M., Curran, M., Das, S. B., Edwards, R., Isaksson, E., Kawamura, K., Kipfstuhl, S., Krüger, K., Layman, L., Maselli, O. J. Motizuki, Y., Motoyama, H., and Pasteris, D. R.: Insights from Antarctica on volcanic forcing during the Common Era, Nat. Clim. Change, 4, 693–697, doi:10.1038/nclimate2293, 2014.

Sigl, M., Winstrup, M., McConnell, J. R., Welten, K C., Plunkett, G., Ludlow, F., Büntgen, U., Caffee, M., Chellman, N., Dahl-Jensen, D., Fischer, H., Kipfstuhl, S., Kostick, C., Maselli, O. J., Mekhaldi, F., Mulvaney, R., Muscheler, R., Pasteris, D. R., Pilcher, J. R., Salzer, M., Schüpbach, S., Steffensen, J. P., Vinther, B. M., and Woodruff, T. E.: Timing and climate forcing of volcanic eruptions for the past 2,500 years, Nature, 523, 543–549, doi:10.1038/nature14565, 2015.

SPARC: SPARC Assessment of Stratospheric Aerosol Properties (ASAP). Thomason, L., and Peter, T., (Eds.), SPARC Report No. 4, WCRP-124, WMO/TD - No. 1295, 2006.

Stoffel, M., Khodri, M., Corona, C., Guillet, S., Poulain, V., Bekki, S., Guiot, J., Luckman, B. H., Oppenheimer, C., Lebas, N., Beniston, M. and Masson-Delmotte, V.: Estimates of volcanic induced cooling in the Northern Hemisphere over the past 1,500 years, Nat. Geosci., 8, 784–788, doi:10.1038/ngeo2526, 2015.

Timmreck, C., Lorenz, S. J., Crowley, T. J., Kinne, S., Raddatz, T. J., Thomas, M. A., and Jungclaus, J. H.: Limited temperature response to the very large AD 1258 volcanic eruption, Geophys. Res. Lett., 36(21), doi:10.1029/2009GL040083, 2009.

Toohey, M., Krüger, K., and Timmreck, C.: Volcanic sulfate deposition to Greenland and Antarctica: A modeling sensitivity study, J. Geophys. Res.-Atmos., 118(10), 4788–4800, doi: 10.1002/jgrd.50428, 2013.

Toohey, M., Stevens, B., Schmidt, H., and Timmreck, C.: Easy Volcanic Aerosol (EVA v1.0): an idealized forcing generator for climate simulations, Geosci. Model Dev., 9, 4049-4070, doi:10.5194/gmd-9-4049-2016, 2016.

5   Toohey, M. and Sigl, M.: Volcanic stratospheric sulphur injections and aerosol optical depth from 500 BCE to 1900 CE, Earth Syst. Sci. Data Discuss., in review, 2017

Trepte, C. R., and Hitchman, M. H.: Tropical stratospheric circulation deduced from satellite aerosol data, Nature, 355(6361), 626–628, 1992.

Trepte, C. R., Veiga, R. E., and McCormick, M. P.: The poleward dispersal of Mount Pinatubo volcanic aerosol, J. Geophys.
10   Res.-Atmos., 98(D10), 18563–18573, doi:10.1029/93JD01362, 1993.

Wolff, E. W.: Chemical signals of past climate and environment from polar ice cores and firn air, Chem. Soc. Rev. Chem. Soc. Rev, 41(41), 6247–6258, doi:10.1039/c2cs35227c, 2012.

Wolff, E. W., Cook, E., Barnes, P. R. F., and Mulvaney, R.: Signal variability in replicate ice cores, J. Glaciol., 51(174), 462–468, doi:10.3189/172756505781829197, 2005.

15   Zanchettin, D., Khodri, M., Timmreck, C., Toohey, M., Schmidt, A., Gerber, E. P., Hegerl, G., Robock, A., Pausata, F. S. R., Ball, W. T., Bauer, S. E., Bekki, S., Dhomse, S. S., LeGrande, A. N., Mann, G. W., Marshall, L., Mills, M., Marchand, M., Niemeier, U., Poulain, V., Rozanov, E., Rubino, A., Stenke, A., Tsigaridis, K., and Tummon, F.: The Model Intercomparison Project on the climatic response to Volcanic forcing (VolMIP): experimental design and forcing input data for CMIP6, Geosci. Model Dev., 9, 2701-2719, doi:10.5194/gmd-9-2701-2016, 2016.

20   Zielinski, G. A.: Stratospheric loading and optical depth estimates of explosive volcanism over the last 2100 years derived from the Greenland Ice Sheet Project 2 ice core, J. Geophys. Res., 100(D10), 20937, doi:10.1029/95JD01751, 1995.

Zielinski, G. A., Mayewski, P. A., Meeker, L. D., Whitlow, S., and Twickler, M. S.: A 110,000-Yr Record of Explosive Volcanism from the GISP2 (Greenland) Ice Core, Quaternary Res., 45(2), 109–118, doi:10.1006/qres.1996.0013, 1996.

25   Zielinski, G.A., Mayewski, P.A., Meeker, L.D., Grönvold, K., Germani, M.S., Whitlow, S., Twickler, M.S. and Taylor, K.: Volcanic aerosol records and tephrochronology of the Summit, Greenland, ice cores, J. Geophys. Res.-Oceans, 102(C12), 26625-26640, doi:10.1029/96JC03547, 1997.

Figures
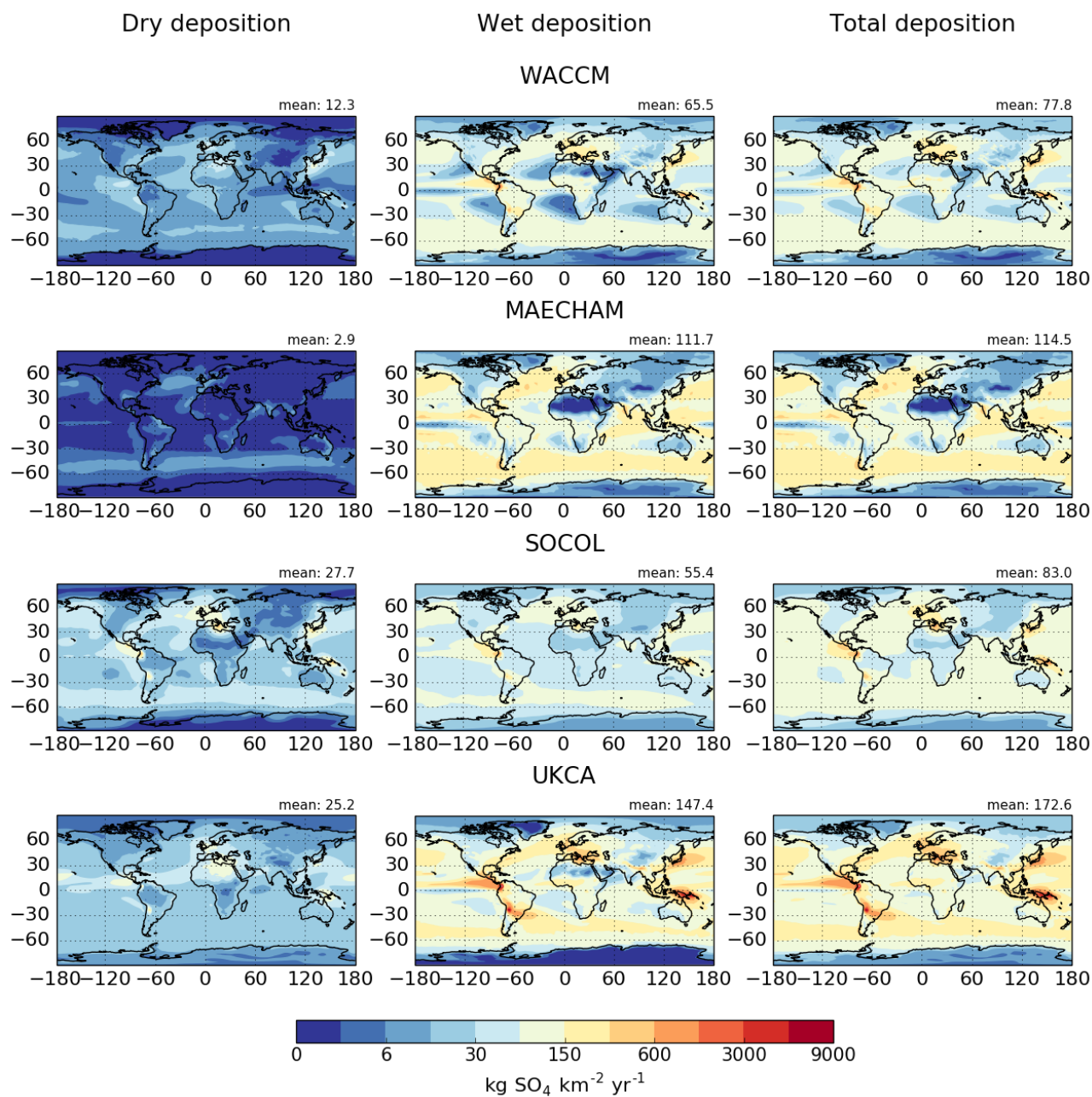
Figure 1: Pre-industrial background annual mean dry, wet and total (wet + dry) sulfate deposition fluxes [kg SO$_4$ km^{-2} yr^{-1}] (left to right) for each model (top to bottom). UKCA is an average of 4 years; MAECHAM and WACCM are averages of 5 years and SOCOL is an average of 1 year due to the length of available simulation. The value shown in the top right-hand corner of each plot refers to the global mean sulfate deposition flux.
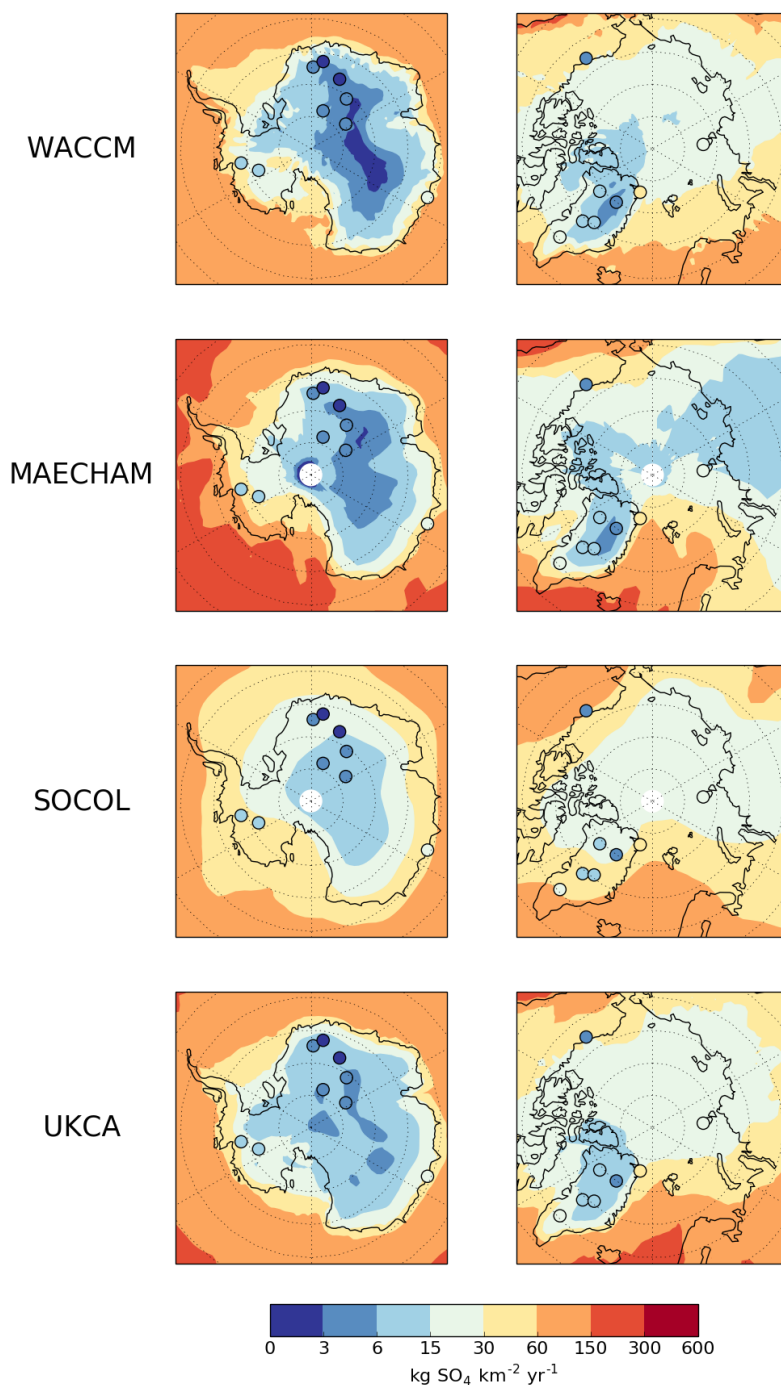
Figure 2: Annual mean total (wet + dry) sulfate deposition fluxes [kg SO$_4$ km^{-2} yr^{-1}] for Antarctica (left) and the Arctic (right) for the pre-industrial background control simulations (shading) compared to pre-industrial ice core sulfate fluxes (filled circles), averaged for 1850 to 1860.
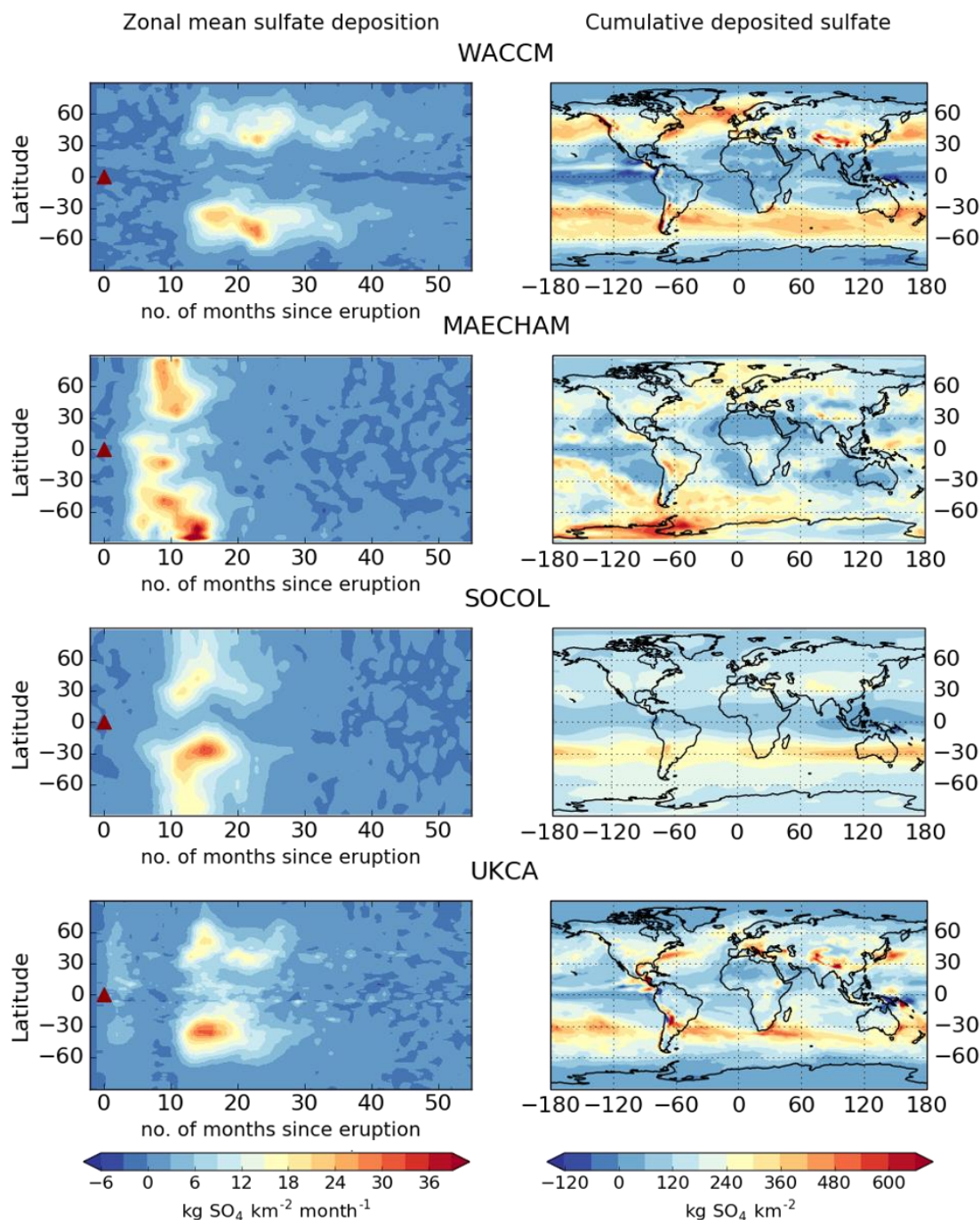
Figure 3: Zonal mean monthly-mean volcanic sulfate deposition [kg SO$_4$ km^{-2} month^{-1}] (left) and cumulative deposited sulfate [kg SO$_4$ km^{-2}] (right) for each model (ensemble mean). The red triangle marks the start of the eruption (1 April 1815). Volcanic sulfate deposition is calculated as the difference in total sulfate deposition (wet + dry) between the perturbed and control simulations and this anomaly is summed over the ~5 years of simulation to produce the cumulative sulfate deposition maps (right column).
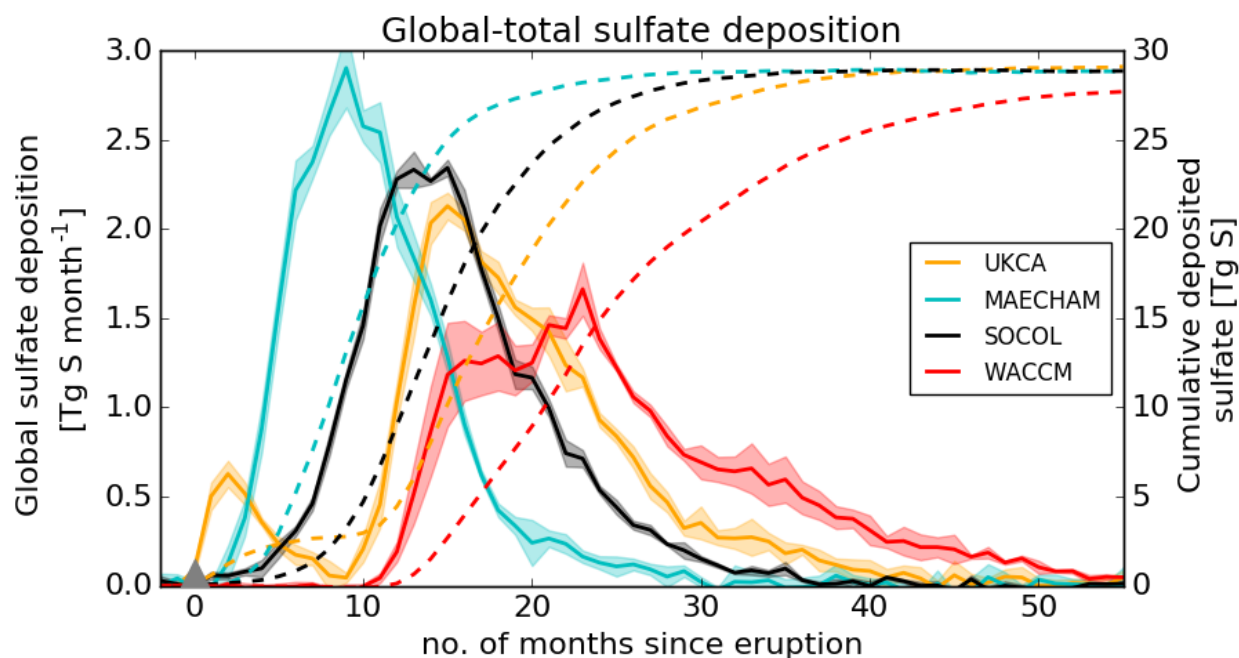
Figure 4: Global-total volcanic sulfate deposition [Tg S month^{-1}] (solid lines – left axis) and global-total cumulative deposited sulfate [Tg S] (dashed lines - right axis) for each model (colours). Ensemble mean is shown by the solid line; shading marks one standard deviation. The grey triangle marks the start of the eruption (1 April 1815).
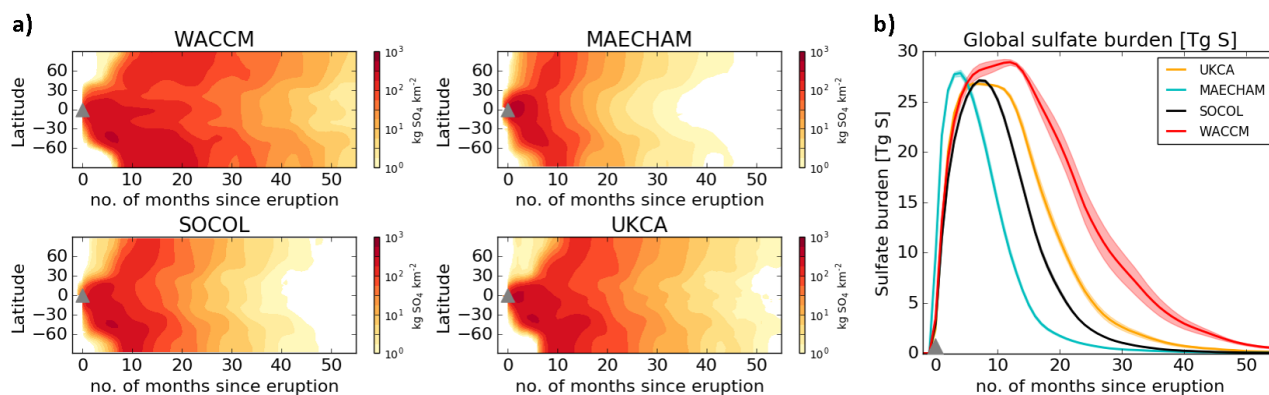
Figure 5: a) Zonal-mean monthly-mean atmospheric sulfate burdens in each model [kg SO$_4$ km^{-2}] b) Global-total atmospheric sulfate burdens [Tg S] for each model (colours). Ensemble means are shown by the coloured lines; shadings mark one standard deviation. The grey triangle marks the start of the eruption (1 April 1815).
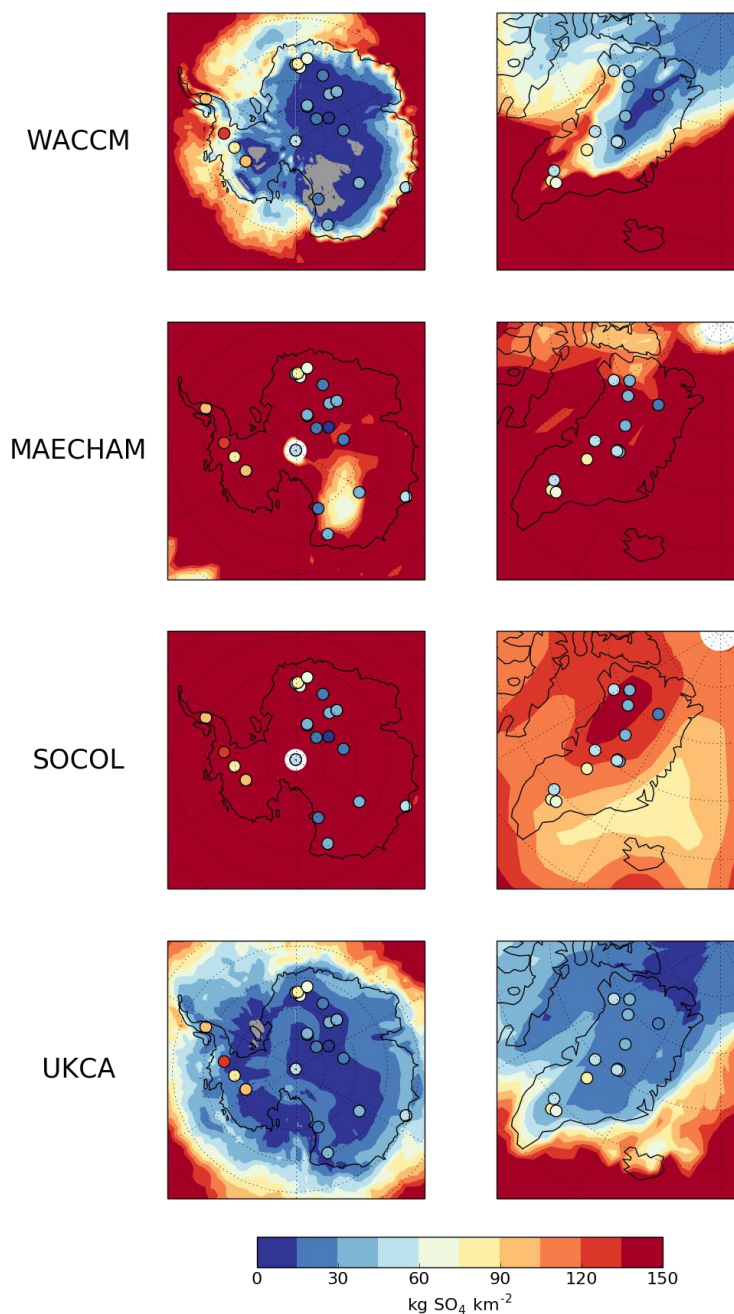
Figure 6: Cumulative deposited sulfate [kg SO$_4$ km^{-2}] integrated over the whole duration of model simulation (~5 years) on Antarctica (left) and Greenland (right) for each model (ensemble mean). Ice core cumulative deposited sulfate values are plotted as coloured circles. Scaled versions for MAECHAM and SOCOL are included in the supplementary information (Fig. S5).
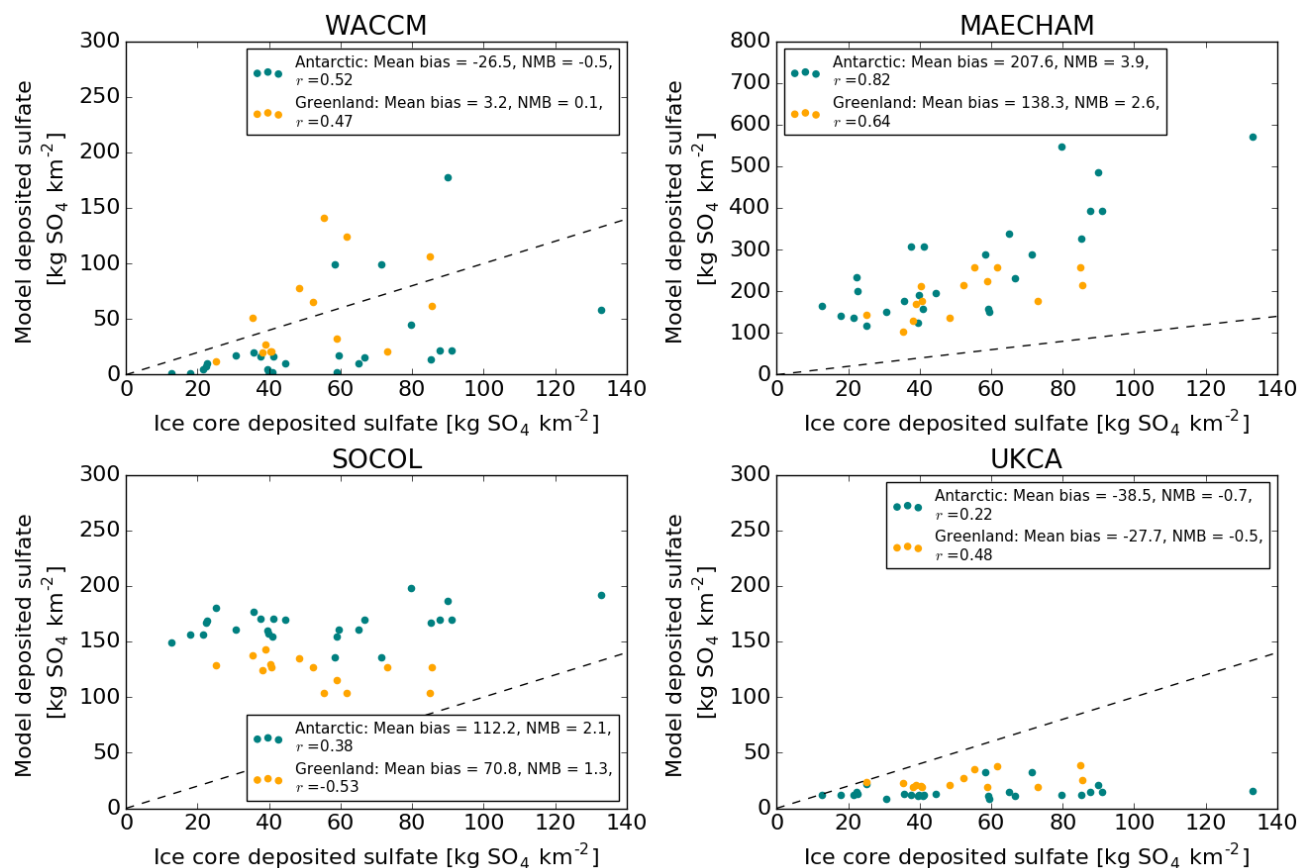
Figure 7: Scatter plots of cumulative deposited sulfate [kg SO$_4$ km^{-2}] due to the eruption of Mt. Tambora recorded in ice cores vs. that simulated by each model (ensemble mean) in Antarctica (teal points) and Greenland (orange points). Simulated values represent the grid box value where each ice core is located. The dashed line marks the 1:1 line. For each model and for Greenland and Antarctica the mean bias, normalized mean bias (NMB) and correlation coefficient (*r*) between the simulated deposited sulfate and ice core values are shown in the legend. Note the increased y-axis scale for MAECHAM.
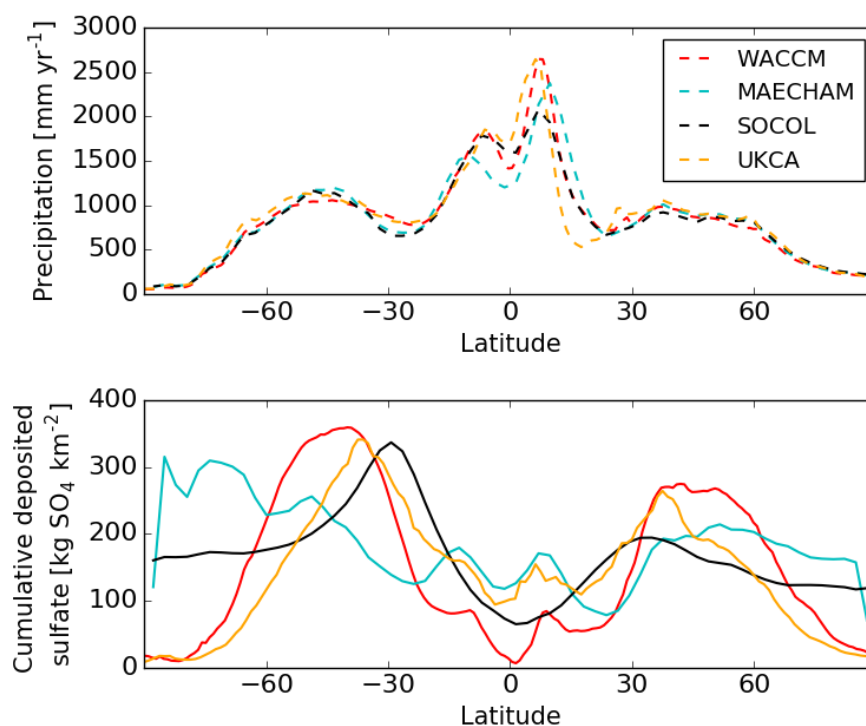
Figure 8: Zonal mean precipitation [mm yr^{-1}] averaged over the first 4 years after the eruption (top panel, dashed lines) and zonal mean cumulative deposited sulfate [kg SO$_4$ km^{-2}] in the first 4 years after the eruption bottom panel, solid lines) in each model (colours).
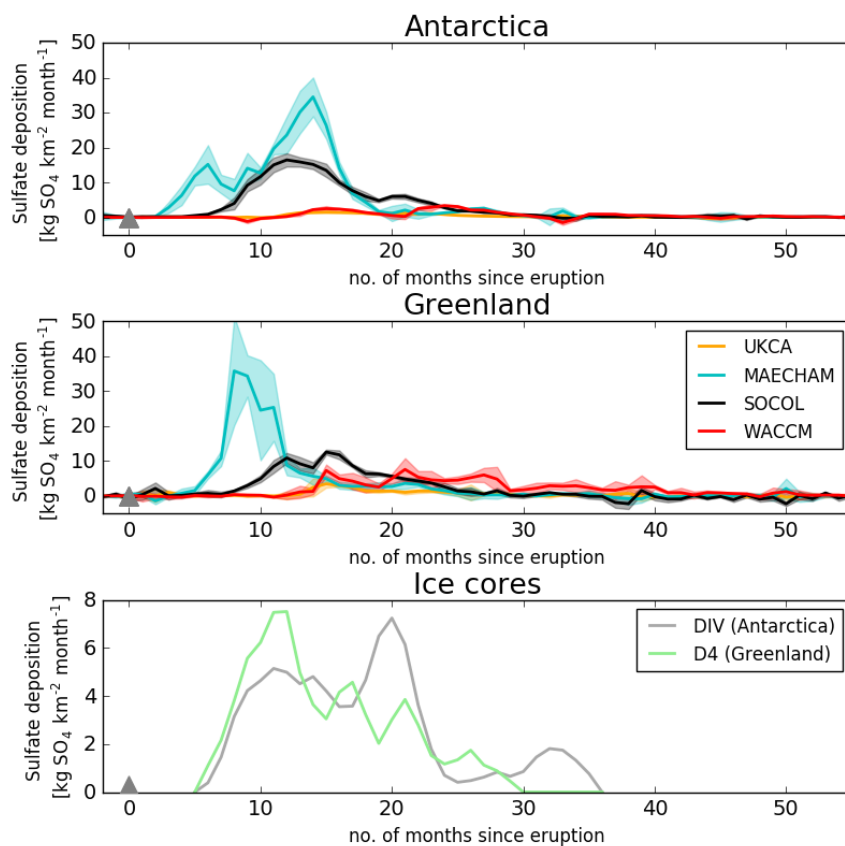
Figure 9: Simulated area-mean volcanic sulfate deposition [kg SO$_4$ km^{-2} month^{-1}] to the Antarctic ice sheet (top panel) and Greenland ice sheet (middle panel) for each model (colours). Solid lines mark the ensemble mean and shading is one standard deviation. In the bottom panel are deposition fluxes from two monthly resolved ice cores (DIV from Antarctica and D4 from Greenland). Note the reduced scale for the bottom panel. The grey triangles mark the start of the eruption.
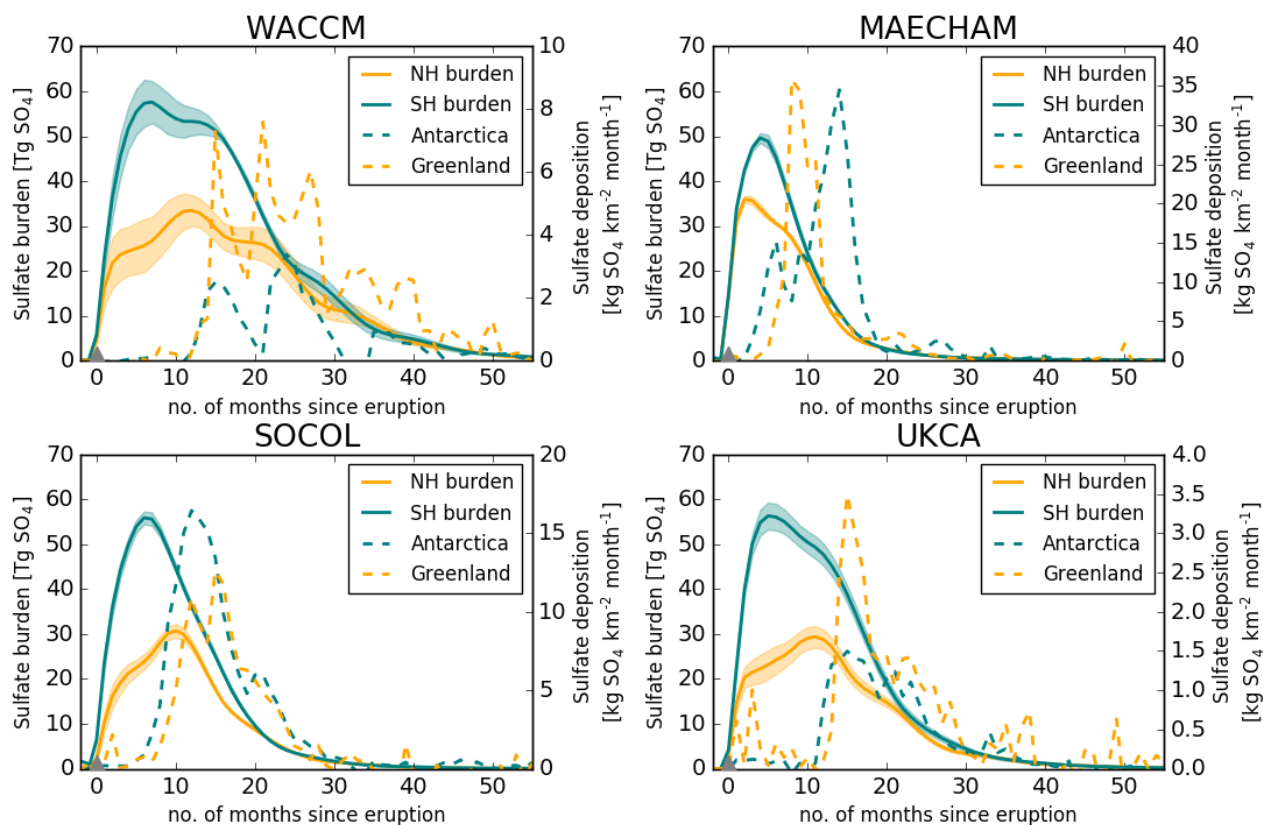
Figure 10: Hemispheric atmospheric sulfate burdens [Tg SO$_4$] (solid lines – ensemble mean, shading is one standard deviation) and area-mean ice sheet volcanic sulfate deposition (dashed lines) [kg SO$_4$ km^{-2} month^{-1}] for each model. The grey triangles mark the start of the eruption. There are different scales on each secondary y axis for ice sheet deposition.
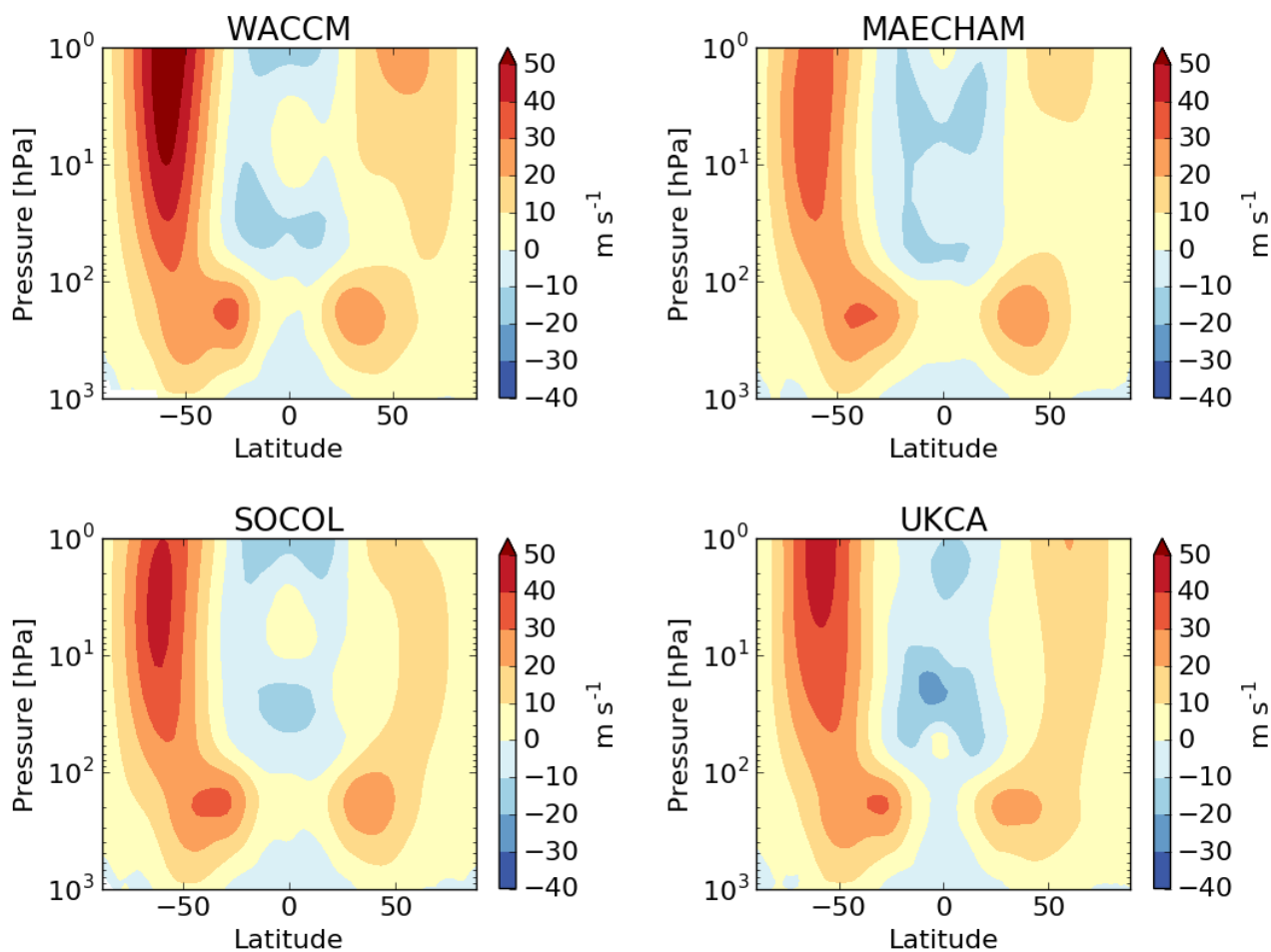
Figure 11: Zonal mean zonal wind [m s^{-1}] averaged over the first year after the eruption (April 1815 – April 1816) in each model simulation (ensemble mean). Zonal wind is output on 36 pressure levels in UKCA, 33 pressure levels in MAECHAM and 32 pressure levels in SOCOL. Zonal wind in WACCM is output on an atmosphere hybrid sigma pressure coordinate and has been interpolated to the pressure levels used in UKCA.

Tables

Table 1: Description of models. In the remaining text model names have been truncated to the section in bold. Modal vs. sectional aerosol size distributions are described in the text.

Model	Horizontal resolution	Model top, model levels	Size distribution	Reference
CESM1(**WACCM**)	0.94°×1.25°	4.5×10^{-6} hPa, 70 levels	modal, 3 modes	Mills et al. (2016)
MAECHAM5-HAM	2.8°×2.8° (T42)	0.01 hPa, 39 levels	modal, 7 modes	Niemeier et al. (2009)
SOCOL-AER	2.8°×2.8° (T42)	0.01hPa, 39 levels	sectional, 40 size bins	Sheng et al. (2015)
UM-**UKCA**	1.25°×1.875° (N96)	84 km, 85 levels	modal, 7 modes	Dhomse et al. (2014)

Table 2: Model parameters used for the Tambora simulations.

Parameter	Value in this study
SO_2 emission	60 Tg SO_2
Eruption length	24 hours
Eruption date	1 April
Latitude	Equator
QBO phase	Easterly
SO_2 injection height	22-26 km*

*Injection differed slightly between the models: SOCOL's SO_2 emission flux was between 22-26 km, increasing linearly with height from zero at 22 km to max at 24 km, and then decreasing linearly to zero at 26 km. MAECHAM injected at a single model level at 30 hPa (~24 km). UKCA used a uniform injection between 22-26 km. WACCM also emitted SO_2 uniformly between 22-26 km, however the overlap of

5 model levels with the emission altitude range resulted in emission fluxes peaking in the centre of the plume, similar to SOCOL.

Table 3: Annual global-total deposition fluxes of SO$_2$, SO$_4$ and SO$_X$ (SO$_2$ + SO$_4$) for dry deposition, wet deposition and total dry + wet (Tg S yr^{-1}) in the pre-industrial controls and in the ACCMIP multi-model mean (see text).

Model	Dry SO$_2$	Wet SO$_2$	Total SO$_2$	Dry SO$_4$	Wet SO$_4$	Total SO$_4$	Dry SO$_X$	Wet SO$_X$	Total SO$_X$
WACCM	5	11	16	2	11	13	7	22	29
MAECHAM	2	2	4	0.5	19	19	3	21	24
SOCOL	10	10	20	5	9	14	15	19	34
UKCA	7	5	12	4	25	29	11	30	41
ACCMIP multi-model mean	-	-	-	-	-	-	11	23	34

Table 4: Global-total cumulative deposited sulfate [Tg S] from dry and wet processes for each model (ensemble mean).

Model	Dry deposition	Wet deposition	Total deposition
WACCM	2.4	25.4	27.8
MAECHAM	0.2	28.6	28.8
SOCOL	0.8	28.0	28.9
UKCA	3.7	25.4	29.1

Table 5: Greenland and Antarctica ice sheet mean cumulative deposited sulfate and ratio (Antarctica deposition/Greenland deposition) and peak NH and SH sulfate burdens (total atmospheric column burden anomaly) and ratio (SH burden/NH burden) for each model (ensemble mean). Also included is the equivalent mean deposited sulfate on each ice sheet calculated from ice cores (Gao et al., 2007; Sigl et al., 2015).

Model	Mean Antarctica deposited sulfate [kg SO$_4$ km^{-2}]	Mean Greenland deposited sulfate [kg SO$_4$ km^{-2}]	Antarctica/ Greenland deposition ratio	Peak SH sulfate burden [Tg SO$_4$]	Peak NH sulfate burden [Tg SO$_4$]	SH/NH burden ratio
WACCM	36	109	0.3	58	34	1.7
MAECHAM	264	194	1.4	50	36	1.4
SOCOL	170	115	1.5	56	31	1.8
UKCA	19	31	0.6	56	29	1.9
Sigl et al., 2015	46	40	1.2	-	-	-
Gao et al., 2007[*]	51	59	0.9	-	-	-

5 *aerosol reported 75:25% H$_2$SO$_4$:H$_2$O

Table 6: Burden-to-Deposition (BTD) factors [* 10^9 km^{-2}] between the hemispheric peak sulfate burden [Tg SO$_4$] (total atmospheric column burden anomaly) and the mean ice sheet cumulative deposited sulfate [kg SO$_4$ km^{-2}] for the four models and from Gao et al. (2007). Included are the values for the ensemble mean factor and the range from individual ensemble members.

Model	NH_BTD [10^9 km^{-2}]		SH_BTD [10^9 km^{-2}]	
	Ensemble mean	Ensemble range	**Ensemble mean**	Ensemble range
WACCM	0.31	0.29-0.34	1.63	1.44-1.96
MAECHAM	0.19	0.14-0.24	0.19	0.17-0.20
SOCOL	0.27	0.25-0.29	0.33	0.31-0.35
UKCA	0.97	0.74-1.14	2.91	2.67-3.30
Multi-model mean	**0.44**	**-**	**1.26**	**-**
Gao et al. (2007)	1	-	1	-